1 # An investigation into atmospheric nitrous acid (HONO)
2 # processes in South Korea

3

4 **Kiyeon Kim[1], Kyung M. Han[1*], Chul H. Song[1*], Hyojun Lee[1], Ross Beardsley[2], Jinhyeok**
5 **Yu[1], Greg Yarwood[2], Bonyoung Koo[3], Jasper Madalipay[1], Jung-Hun Woo[4], and Seogju**
6 **Cho[5]**

7

8   1. School of Earth Sciences and Environmental Engineering, Gwangju Institute of Science and
9   Technology (GIST), Gwangju 61005, Republic of Korea

10 2. Ramboll USA, Novato, CA 94945, USA

11 3. Bay Area Air Quality Management District, San Francisco, CA 94105, USA

12 4. Department of Technology Fusion Engineering, College of Engineering, Konkuk University,
13   Seoul 05029, Republic of Korea

14 5. Seoul Metropolitan Government Research Institute of Public Health Environment, 30,
15   Janggunmaeul 3-gil, Gwacheon-si, Gyeonggi-do 13818, Republic of Korea

16

17

18 **Short title:** Atmospheric HONO processes

19

20 * **Corresponding authors:** Kyung Man Han (kmhan@gist.ac.kr) and Chul Han Song

21 (chsong@gist.ac.kr)

22

23 (Submitted to *Atmospheric Chemistry and Physics*)

24   **Abstract**

25   Nitrous acid (HONO) is a main precursor of hydroxyl radicals (OH), which contribute

26   to the formation of numerous secondary air pollutants in the troposphere. Despite its

27   importance in atmospheric chemistry, HONO chemistry has not been fully incorporated into

28   many chemical transport models (CTMs). Due to the lack of atmospheric HONO processes,

29   CTM simulations often tend to underestimate atmospheric mixing ratios of HONO. This study

30   was undertaken because simulations with current Community Multiscale Air Quality (CMAQ)

31   model have a strong tendency to underestimate the HONO mixing ratio. In search of missing

32   sources of atmospheric HONO, we attempted to sequentially incorporate the following

33   potential HONO sources and processes into the CMAQ modeling framework: (i) gas-phase

34   HONO reactions; (ii) traffic HONO emissions; (iii) soil HONO emissions; (iv) heterogeneous

35   HONO production on the surfaces of aerosols; (v) heterogeneous HONO formation on tree leaf

36   and building surfaces; (vi) photolysis reactions of particulates and deposited HNO_3/nitrates

37   called 'renoxification'. The simulation performances of the modified CMAQ models were then

38   evaluated by comparing the modeled HONO mixing ratios with the HONO mixing ratios

39   observed at the Olympic Park station in Seoul, South Korea. When HONO processes were fully

40   added to the CMAQ model, average daily HONO mixing ratios increased from 0.06 ppb to

41   1.18 ppb. The daytime HONO mixing ratios produced from the CMAQ model run with a full

42   account of atmospheric HONO processes were found to be in better agreement with

43   observations than those from the original CMAQ model (CMAQv5.2.1) runs with improved

44   statistical metrics (e.g., IOA increased from 0.59 to 0.68, while MB decreased dramatically

45   from -0.57 ppb to -0.34 ppb). In addition, we investigated the contributions of individual

46   atmospheric HONO processes to HONO mixing ratios, as well as the impacts of HONO

47   atmospheric processes on the concentrations of other atmospheric species in South Korea. All

48   these issues are also discussed in this manuscript.

2

49   **Keywords**: Nitrous acid (HONO); Heterogeneous HONO production; CMAQ model; Ozone
50   production rate.

1. Introduction

Hydroxyl radicals (OH) play a key role in atmospheric chemistry. OH radicals oxidize volatile organic compounds (VOCs), sulfur dioxide (SO_2), and nitrogen dioxide (NO_2), contributing to the formation of secondary organic and inorganic aerosols (Pathak et al., 2009). Therefore, accurate determination of the mixing ratio of OH radicals is crucial to understanding atmospheric photochemistry in both polluted and remote areas.

Nitrous acid (HNO_2 or HONO) has been recognized as a main precursor of OH radicals via photo-dissociation (R1) (Alicke et al., 2003; Harris et al., 1982; Kleffmann et al., 2005):

$$HONO + hv \xrightarrow{j_{HONO}} OH + NO \ (300 \ nm < \lambda < 405 \ nm) \tag{R1}$$

Several studies have estimated that HONO photolysis reactions contribute 20 – 80% of OH radicals and 30 – 87% of HO_x formation in polluted urban areas (Acker et al., 2006; Alicke et al., 2003; Hendrick et al., 2014; Kim et al., 2014; Kleffmann et al., 2005; Monks et al., 2009; Ren et al., 2003). However, it was also recognized that the HONO chemistry was not yet fully understood.

Therefore, many field measurements have been carried out to characterize atmospheric HONO processes (Kim et al., 2014; Lee et al., 2016; Li et al., 2012; Su et al., 2008). These studies showed that the observed HONO mixing ratios were significantly higher than those predicted by atmospheric chemistry-transport model simulations (Lee et al., 2016; Li et al., 2014; Su et al., 2008; VandenBoer et al., 2013). This indicates that there should be missing HONO sources or processes that are not considered in current atmospheric models (CTMs).

Recent studies have proposed incorporating several HONO production pathways into chemical transport models to explain the missing HONO processes. Suggested sources include i) traffic HONO emissions (Czader et al., 2015; Kirchstetter et al., 1996; Kurtenbach et al., 2001; Li et al., 2018; Nakashima and Kajii, 2017; Rappenglück et al., 2013; Xu et al., 2015);

4

75 ii) soil HONO emissions (Meusel et al., 2016; Nagai and Kubota, 1972; Oswald et al., 2013;

76 Weber et al., 2015); iii) HONO emissions from biomass burning (Cheng et al., 2014; Crutzen

77 and Andreae, 1990; Nie et al., 2015); iv) indoor HONO emissions (Gligorovski, 2016; Zhang

78 et al., 2019); and iv) heterogeneous conversion of NO_2 to HONO on the surfaces of aerosols,

79 grounds, and leaves (Han et al., 2017; Reisinger, 2000; Svensson et al., 1987; Stemmler et al.,

80 2016; Wiesen et al., 1995).

81   Among these processes, traffic HONO emissions were reported to be the key factor

82 influencing the HONO mixing ratio in the Beijing–Tianjin–Hebei (BTH) region at night

83 (Zhang et al., 2019). Heterogeneous NO_2 reactions on aerosol surfaces were an important

84 source of HONO during the severe haze period in Beijing (Jia et al., 2020). On the other hand,

85 Zhang et al. (2016) reported that heterogeneous reactions on ground surfaces could be the

86 dominant source of atmospheric HONO, accounting for ~42% of the HONO mixing ratios in

87 Hong Kong suburban areas.

88   These findings may indicate that atmospheric HONO production and a potential cause

89 of discrepancies between modeled and observed HONO mixing ratios may vary temporally

90 and regionally. In addition, no research has been conducted on which sources of HONO control

91 the levels of HONO in Seoul, South Korea. In this context, the aims of this study are three-fold:

92 i) to determine which HONO sources or processes are significant in South Korea; ii) to estimate

93 the budget of the HONO mixing ratios from various HONO sources; and iii) achieving

94 objectives i) and ii) to develop a near-perfect CTM in terms of HONO mixing ratio. To

95 accomplish these goals, we decided to improve the US EPA CMAQ v5.2.1 model by

96 incorporating several HONO production pathways including i) homogeneous HONO reactions;

97 ii) direct HONO emissions from biomass burning, traffic vehicles, and soil; iii) heterogeneous

98 HONO production on the surfaces of atmospheric aerosols, buildings, and tree leaves; and iv)

99 photolysis reactions of particulate and deposited HNO_3/nitrate (renoxification).

100   We then tested the performances of the modified CMAQ models by comparing the

101   modeled HONO mixing ratios with the HONO mixing ratios observed during the Korea-United

102   States Air Quality (KORUS-AQ) campaign. After the comparison analysis, we evaluated the

103   contributions of individual HONO processes to the HONO budget in South Korea and also

104   investigated the effects of the HONO mixing ratios on the levels of other important atmospheric

105   species.

106   **2. Methodology**

107   In this study, we incorporated various HONO sources and reactions into the CMAQ

108   model framework to accurately estimate HONO mixing ratios in the atmosphere. Then, the

109   simulation results of the modified CMAQ models were analyzed, comparing the modeled

110   outputs with observations during the KORUS-AQ campaign. Details of the modifications of

111   CMAQ models, the HONO measurements, and potentially important HONO sources

112   considered in this study are described in the following sections.

113   **2.1. WRF-CMAQ model configuration**

114   Simulation of the Community Multiscale Air Quality (CMAQ) v5.2.1 model (Byun

115   and Schere, 2006) was carried out to estimate the HONO mixing ratios during the period of the

116   KORUS-AQ campaign (9 May – 12 June, 2016). Figure 1 shows the horizontal domain (A1)

117   for the CMAQ model simulation. The spatial domain has 273×204 grid cells with a horizontal

118   resolution of 15×15 km^2 and contains 15 vertical layers with the first layer at ~34 m above

119   the ground.

120   The photochemical mechanism used in the simulation of the CMAQ model was the

121   Statewide Air Pollution Research Center-07 (SAPRC-07 TC) (Carter, 2010; Hutzell et al.,

122   2012). The AERO6 module was used for aerosol calculations (Binkowski and Roselle, 2003).

123   In particular, the heterogeneous reactions considered in this study were embedded into the

6

124   SAPRC-07 TC via the Korean Flexible Chemistry (KFC) editor. The KFC editor is a chemical

125   mechanism editor in a framework of Graphic User Interface (GUI) developed to quickly

126   implement the modifications of the chemical mechanisms of the CMAQ model. The details of

127   the heterogeneous reactions we considered are discussed in Sects. 2.3.5 – 2.3.6.

128   The Weather Research and Forecasting (WRF) v3.8.1 model (Skamarock et al., 2008)

129   was run to generate meteorological fields that drive the CMAQ model. The physical options

130   used in the WRF run are as follows: i) WRF Single-Moment 6-class Microphysics scheme

131   (Hong and Lim, 2006); ii) Rapid radiative transfer model (RRTMG) for longwave and

132   shortwave radiation (Iacono et al., 2008); iii) the NOAH Land Surface scheme (Chen and

133   Dudhia, 2001); iv) Yonsei University (YSU) Planetary Boundary Layer (PBL) scheme (Hong

134   et al., 2006); v) MM5 surface layer scheme (Jiménez et al., 2012); and vi) the Grell-Freitas

135   Ensemble scheme for cumulus physics (Grell and Freitas, 2014). Initial and boundary

136   conditions for the WRF model runs were obtained from the National Center for Environmental

137   Prediction Final Analysis (NCEP-FNL) every six hours.

138   For anthropogenic emissions, this study used the KORUS v5.0 inventory processed by

139   the Sparse Matrix Operator Kernel Emissions in Asia (SMOKE-Asia; Woo et al., 2012) (Woo

140   et al., 2020). The KORUS v5.0 emissions were developed particularly for CTM runs as part of

141   the KORUS-AQ campaign. Biogenic emissions were generated using the Model of Emissions

142   of Gases and Aerosol from Nature (MEGAN) v2.10 (Guenther et al., 2012). Fire emissions

143   were obtained from the Fire Inventory from NCAR (FINN) v1.5 emission inventory

144   (https://bai.acom.ucar.edu/Data/fire/; Wiedinmyer et al., 2011). The various HONO emissions

145   considered in this study are discussed in Sects. 2.3.2. – 2.3.4.

146
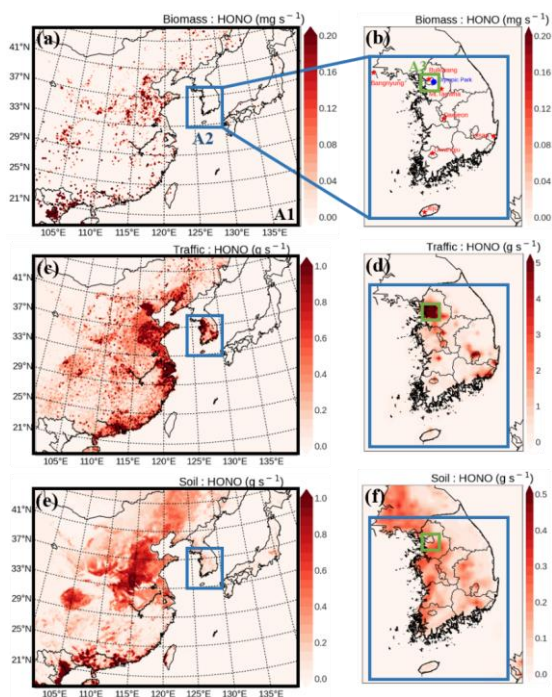
Figure 1. Spatial distributions of HONO emission rates from biomass burning (panels (a) and (b)), from traffic (panels (c) and (d)), and from soil (panels (e) and (f)) over East Asia (A1), South Korea (A2), and the Seoul Metropolitan Area (A3). Several super-monitoring stations are located at Bangnyung-Do, Bulkwang-Dong, Olympic Park, Mt.Taehwa, Daejeon, Gwangju, Ulsan, and Jeju. The locations of these super-stations are shown in panel (b).

2.2 Measurements

During the KORUS-AQ campaign period, concentrations of NO_2, O_3, and particulate matter were measured at several locations such as Olympic Park (37.52N; 127.12E), Bangnyung (37.96N; 124.64E), Bulkwang (37.61N; 126.93E), Mt. Taewha (37.31N; 127.31E), Daejeon (36.35N; 127.38E), Gwangju (35.23N; 126.84E), Ulsan (35.53N; 129.31E), and Jeju (33.32N; 126.40E) (refer to Fig. 1b regarding the locations). In this study, we also used data observed at approximately 320 stations from the AIR-KOREA network (https://www.air.korea.or.kr), officially managed by the Korean Ministry of Environment in South Korea.

8

161 Surface data observed at the Olympic Park station in Seoul were used for direct comparisons

162 between simulated and observed HONO mixing ratios. These HONO mixing ratios were

163 measured using the Monitor for AeRosols and GAses in ambient air (MARGA ADI 2080)

164 (Applikon-ECN, Netherlands) instrument with a time resolution of 1 hour. This measurement

165 is based on the wet-denuder-ion-chromatography (WD/IC) method. In the WD/IC system,

166 HONO molecules absorbed by the solution in the denuder were converted to nitrite (NO_2^-),

167 and then the nitrite concentrations were quantified by ion chromatography (Xu et al., 2019).

168 The detection limit of the MARGA instrument for HONO is ~0.02 ppb. At the Olympic Park

169 station, NO_2 and O_3 were also measured using commercially available instruments, EC9841

170 and EC9810, respectively, manufactured by Ecotech. Their detection limits for both species

171 are ~0.5 ppb during the daytime. Details on the principles of EC9841 and EC9810 can be

172 found in Keywood et al. (2019). $PM_{2.5}$ at the Olympic Park station were measured

173 continuously using a Thermo Scientific Continuous Particulate Monitor, FH62C14, based on

174 the beta attenuation method. The detection limit of the instrument is $4\mu g/m^3$ in hourly

175 measurements. Further information about instruments is provided in Table S1.

176   Meteorological data on temperature, relative humidity, pressure, wind speeds, and

177 wind directions were also measured by the Automated Synoptic Observing System (ASOS) at

178 the Olympic Park station. In order to test the simulation performances of the WRF-CMAQ

179 model, observed meteorological data was compared with the modeled outputs, which is shown

180 in Figure S1 and Table S2. In general, WRF model simulations tended to accurately predict

181 meteorological fields.

9

Table 1. Comparison of parameterizations of HONO processes between CMAQ v5.2.1 and this study.

	HONO processes	CMAQ v5.2.1	This study	Ref.
Reaction	(R1) $HONO + hv \xrightarrow{j_{HONO}} OH + NO$	J_{HONO}	J_{HONO}	1
	(R2) $NPHE + hv \xrightarrow{j_{NPHE}} HONO + xPROD2$	$J_{NPHE} = 1.50e^{-3} \times J_{NO_2}$	$J_{NPHE} = 1.50e^{-3} \times J_{NO_2}$	1
	(R3) $OH + NO + M \xrightarrow{k_3} HONO$	$k_3 = \{\frac{k_a[M]}{(1+k_a[M]/k_b)}\}0.6^{\frac{1}{1+[\log_{10}(\frac{k_a[M]}{k_b})]^2}}$ ▪ $k_a = 7.0 \times 10^{-31}(\frac{T}{300})^{-2.6}$, ▪ $k_b = 3.6 \times 10^{-11}(\frac{T}{300})^{-0.1}$	▪ $k_a = 7.1 \times 10^{-31}(\frac{T}{300})^{-2.6}$, ▪ $k_b = 3.6 \times 10^{-11}(\frac{T}{300})^{-0.1}$	2
	(R4) $HONO + OH \xrightarrow{k_4} H_2O + NO_2$	$k_4 = 2.5 \times 10^{-12}e^{(\frac{-260}{T})}$	$k_4 = 3.0 \times 10^{-12}e^{(\frac{-250}{T})}$	2
	(R5) $2NO_2 + H_2O \xrightarrow{k_{aerosol}} HONO + HNO_3$	$k_{aerosol} = 1.0 \times 10^{-4}(S/V)$	$k_{aerosol} = \frac{1}{4}v_{NO2}(S/V) \times \gamma_{a\_NO_2}$ Daytime: $\gamma_{a\_NO_2} = 1.3 \times 10^{-4} \times \frac{light\ intensity}{900(W\cdot M^{-2})}$ Nighttime: $\gamma_{a\_NO_2} = 8.0 \times 10^{-6}$	3, 4 5
	(R6) $2NO_2 + H_2O \xrightarrow{k_{ground}} HONO + HNO_3$	$k_{ground} = 5.0 \times 10^{-5} \times (\frac{S_{g,building}}{V} + \frac{S_{g,leaf}}{V})$ ▪ $\frac{S_{g,leaf}}{V} = \frac{2\times LAI}{H}$ ▪ $\frac{S_{g,building}}{V} = PURB \times \frac{0.2\frac{m^2}{m^3}}{100\%}$	$k_{ground} = \frac{1}{8} \times V_{NO_2} \times \gamma_{g\_NO_2} \times (\frac{S_{g,building}}{V} + \frac{S_{g,leaf}}{V})$ ▪ $\frac{S_{g,leaf}}{V} = \frac{2\times LAI}{H}$ ▪ $\frac{S_{g,building}}{V} = PURB \times \frac{0.3\frac{m^2}{m^3}}{100\%}$ Daytime: $\gamma_{g\_NO_2} = 5.8 \times 10^{-6} \times \frac{light\ intensity}{900(W\cdot M^{-2})}$ Nighttime: $\gamma_{g\_NO_2} = 5.0 \times 10^{-7}$	6 7 4, 8 9
	(R7) $pNO_3 + hv \xrightarrow{J_{pNO_3}} 0.67HONO + 0.33NO_2$	-	$J_{pNO_3} = 118 \times J_{HNO_3}$	10
	(R8) $Deposited\_HNO_3/nitrate + hv$ $\xrightarrow{J_{D\_HNO_3/nirate}} 0.67HONO + 0.33NO_2$	-	$J_{D\_HNO_3/nirate} = 48 \times J_{HNO_3}$	10
Emission	Biomass Burning	-	FINNv1.5	11
	Traffic	-	Gasoline: $HONO_{traffic}/NO_x = 0.8\%$ Diesel: $HONO_{traffic}/NO_x = 2.3\%$	7
	Soil	-	$HONO_{soil}/NO_x = f(soil\ water\ content)$	12

1. Burkholder et al. (2015); 2. Burkholder et al. (2020); 3. Xue et al. (2022); 4. Czader et al. (2012); 5. Vandenboer et al. (2013); 6. Sarwar et al. (2008); 7. Zhang et al. (2016); 8. Yu et al. (2021); 9. Yu et al. (2022); 10. Fu et al. (2019); 11. Wiedinmyer et al. (2011); 12. Meusel et al. (2018)

184 **2.3 HONO sources**

185   In this study, we considered several possible missing HONO sources or processes in

186 the CMAQ model simulations. The possible missing HONO sources include gas-phase HONO

187 reactions, three HONO emission sources, three heterogeneous HONO reactions, and two

188 photolytic reactions. The considered possible missing HONO sources are also contrasted to the

189 current HONO processes embedded in the CMAQ v5.2.1 model in Table 1. The details of each
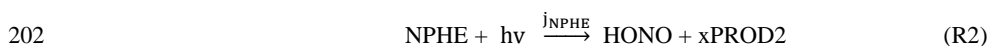
190 HONO process are discussed below.

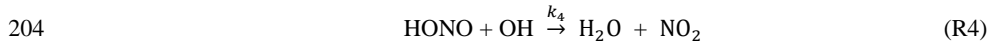191 **Table 2.** Design for 8 EXP simulations.

HONO Source	Experiment							
	EXP1	EXP2	EXP3	EXP4	EXP5	EXP6	EXP7	EXP8
GAS[1]	√	√	√	√	√	√	√	√
BioB[2]		√	√	√	√	√	√	√
TRAF[3]			√	√	√	√	√	√
SOIL[4]			√	√	√	√	√	√
HET_A[5]					√	√	√	√
HET_L[6]						√	√	√
HET_BD[7]							√	√
RENO$_x$[8]								√

192 [1] Gas-phase reactions; [2] Biomass Burning Emissions; [3] Traffic Emissions; [4] Soil Emissions; [5] Heterogeneous reactions on
193 aerosol surfaces; [6] Heterogeneous reactions on the surfaces of leaves; [7] Heterogeneous reactions on the surfaces of buildings;
194 [8] Renoxification

195 **2.3.1 Gas Phase reactions (GAS)**

196   We used the SAPRC-07 TC chemical mechanism as base mechanism. A total of 4 gas-

197 phase HONO-related reactions were considered for HONO formation and dissociation (Carter,

198 2010;). HONO is produced by i) photolysis of nitrophenol (NPHE) (R2) and ii) reaction of

199 NO with OH in the presence of the third body (M) (R3). Meanwhile, HONO is removed by

200 reaction with OH radicals (R4) and photolytic dissociation (R1). All these reactions are shown

201 below:

202 $$NPHE + hv \xrightarrow{j_{NPHE}} HONO + xPROD2 \qquad (R2)$$

203 $$OH + NO + M \xrightarrow{k_3} HONO \qquad (R3)$$

$$\text{HONO} + \text{OH} \overset{k_4}{\rightarrow} \text{H}_2\text{O} + \text{NO}_2 \tag{R4}$$

204
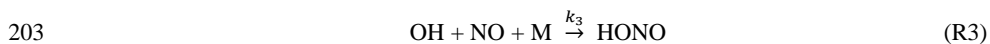
205 where, J_{NPHE} (R2) and J_{HONO} (R1) are the photolysis rates constants of NPHE and HONO,

206 respectively, which were adopted from the study of Stockwell et al. (1990). As shown in Table

207 1, J_{NPHE} was calculated, based on J_{NO2} (i.e., $J_{NPHE} = 1.50 \times 10^{-3} \times J_{NO2}$), which was defined

208 in Bejan et al. (2006). k_3 and k_4 are the reaction rate constants of (R3) and (R4) and were

209 obtained from the National Aeronautics and Space Administration (NASA) Jet Propulsion

210 Laboratory (JPL) Publication 19 (Burkholder et al., 2020). Among these reactions, the reaction

211 rate constants of (R3) and (R4) were updated in our study (refer to Table 1). The effect of these

212 gaseous reactions on HONO mixing ratios was tested in the EXP1 simulation (see GAS in

213 Table 2).

214 **2.3.2 Biomass burning emissions (BioB)**

215 Biomass combustion includes three types of burning events: natural wildfires,

216 agricultural fires, and wood burning (Wiedinmyer et al., 2011). In East Asia, agricultural fires

217 typically occur in early summer and fall (Ryu et al., 2004; Tao et al., 2013; Zhang et al., 2013).

218 The period of the KORUS-AQ campaign coincides with the period of the agricultural residue

219 burning after barley and wheat harvest in East Asia. Biomass burning emissions, including

220 agricultural fire emissions, were obtained from the Fire INventory from NCAR version 1.5

221 (FINN v1.5, Wiedinmyer et al., 2011; Wiedinmyer et al., 2006). This was then considered in

222 the EXP2 simulation (see BioB in Table 2). The spatial distributions of HONO emissions from

223 the biomass burning events in the East Asia domain (A1), South Korea domain (A2), and Seoul

224 Metropolitan Area domain (A3) are presented in Fig. 1a and 1b. However, we found that the

225 HONO emission rates used in the EXP2 simulation were relatively small, compared to the total

226 HONO emission rates presented in Fig. 1 and Table 3.

227

12

228

Table 3. HONO emission rates from biomass burning, traffic, and soil. The total HONO emission rates during the period of the KORUS-AQ campaign are shown.

Region	Source			
	Biomass Burning Emission $(g \cdot s^{-1})$	Traffic Emission $(Mg \cdot s^{-1})$	Soil Emission $(Mg \cdot s^{-1})$	Total $(Mg \cdot s^{-1})$
East Asia (A1)	2.46	6.40	5.65	14.51
South Korea (A2)	0.00	0.32	0.06	0.38
Seoul Metropolitan Area (A3)	0.00	0.10	0.01	0.1

2.3.3 Traffic emissions (TRAF)

Traffic emissions are an important HONO source, particularly at night (Zhang et al., 2016). HONO is emitted directly from vehicle exhaust systems. In this study, to estimate the direct HONO emissions from traffic sources, we assumed that the HONO to NO_x emission ratio is 0.8% for gasoline vehicles and 2.3% for diesel vehicles (Sarwar et al., 2008; Zhang et al., 2016). All off-road vehicles were treated as diesel vehicles in the calculations of HONO emissions (Gutzwiller et al., 2002). Table 3 presents the total emission rates for East Asia, South Korea, and the Seoul Metropolitan Area, which are 6.40, 0.32, and 0.1 Mg s^{-1}, respectively. Moreover, as shown in Fig. 1c and 1d, HONO emissions from traffic sources are dominant, particularly in metropolitan areas such as Seoul, Beijing, Shanghai, and Hong Kong. The contribution of traffic sources to total HONO emissions was estimated to be dominant in the Seoul Metropolitan Area. In the EXP3 simulation, the impact of the traffic source (see TRAF in Table 2) on the atmospheric HONO mixing ratios was investigated.

2.3.4 Soil emissions (SOIL)

Emissions from soil bacterial activity are important sources of HONO. The amount of their emissions depends on the soil type, land category, fertilization, temperature, soil water

13

247 content (SWC in %), and soil pH (Meusel et al., 2018; Wu et al., 2020). In this study, HONO

248 emissions were estimated based on the ratio of HONO to NO_x emissions from soil (Oswald et

249 al., 2013). SWC was used as a proxy for soil pH due to the technical limitations of direct

250 measurement of the soil pH. The SWCs were set at 0-7.5%, 7.5-15%, 15-20%, 20-30% and 30-

251 40% for HONO-to-NO_x ratios of 1.0, 0.67, 0.75, 0.5 and 0.25, respectively, because the ratio

252 of HONO to NO_x is very sensitive to the water content in the soil. For this estimation, monthly

253 soil NO_x emissions were acquired from the MEGAN v2.10 model.

254   The HONO emission rate from soil was estimated at 0.06 Mg s^{-1} for South Korea,

255 accounting for ~16% of the total HONO emission rate in South Korea (refer to Table 3). The

256 spatial distributions of emission are presented in Fig. 1e and 1f. The impact of HONO soil

257 emissions (see SOIL in Table 2) was examined in the EXP4 simulation.

2.3.5 Heterogeneous reaction of NO_2 on atmospheric aerosol surfaces (HET_A)

259   In the EXP5 simulation, we added the heterogeneous reaction of NO_2 on the surface of

260 atmospheric aerosols via reaction (R5) (see HET_A in Table 2), which has been reported to be

261 a possible pathway for HONO formation (Han et al., 2017; Lu et al., 2018; Reisinger, 2000;

262 Svensson et al., 1987; Wiesen et al., 1995).

$$2NO_2 + H_2O \xrightarrow{k_{aerosol}} HONO + HNO_3 \qquad (R5)$$
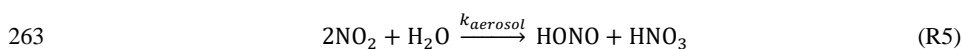
264   We found a similar diurnal pattern of the concentration ratio of HONO/NO_2 to the

265 HONO mixing ratio at the Olympic Park station. This indicates that the conversion of NO_2 to

266 HONO via reaction (R5) may be a main process for HONO formation (Fig. S2Fig. S1). The

267 HONO/NO_2 ratios at the Olympic Park station in Seoul ranged from 1.9% to 6.8% during the

268 KORUS-AQ campaign, which is also comparable to those observed in Taichung, Taiwan, and

269 Shanghai, China (Hao et al., 2020; Tong et al., 2015).

14

270   The current AERO6 module in the CMAQv5.2.1 model already considers reaction (R5)

271   but does not take into account 'photo-enhancement'. However, several previous studies

272   suggested that the photo-enhanced reactions should produce more HONO molecules during the

273   daytime (Colussi et al., 2013; Czader et al., 2012; Fu et al., 2019; Levy et al., 2014; Li et al.,

274   2010; Sarwar et al., 2008). The potential photo-enhancement of the reaction (R5) was taken

275   into account by making $k_{aerosol}$ dependent on the magnitude of light intensity:

276    $$k_{aerosol} = \frac{1}{4} \times v_{NO_2} \times \frac{S_{aero}}{V} \times \gamma_{a,NO_2} \qquad \text{(Eq.1)}$$

277    $$\gamma_{a,NO_2} = 8.0 \times 10^{-6} \quad \text{(nighttime)}$$

278    $$\gamma_{a,NO_2} = 1.3 \times 10^{-4} \times \left(\frac{light\ intensity}{900}\right) \quad \text{(daytime)}$$

279   where, v_{NO_2}, $\frac{S_{aero}}{V}$, and γ_{a,NO_2} represent the mean molecular velocity of NO_2 $(m \cdot s^{-1})$, the

280   aerosol surface density $(m^2 \cdot m^{-3})$, and the NO_2 uptake coefficient on the surface of

281   atmospheric aerosols, respectively. The values of γ_{a,NO_2} were finally selected from the

282   sensitivity tests. It should also be noted in Table 1 that the CMAQ v5.2.1 model simply uses a

283   fixed reaction constant $(= 10^{-4} \times \frac{S_{aero}}{V})$ for this heterogeneous reaction.

2.3.6 Heterogeneous reactions of NO$_2$ on tree leaf and building surfaces (HET_L and

HET_BD)

286   The heterogeneous reaction of NO_2 can also take place on the ground surfaces (e.g.,

287   tree leaves and buildings). Several studies have reported that heterogeneous reactions on the

288   surfaces of tree leaves and buildings via reaction (R6) can contribute to the HONO mixing

289   ratios in the atmosphere (An et al., 2013; Hou et al., 2016; Karamchandani et al., 2015; Zhang

290   et al., 2016). Therefore, we also considered these photo-enhanced heterogeneous NO_2 reactions.

291    $$2NO_2 + H_2O \xrightarrow{k_{L\&B}} HONO + HNO_3 \qquad \text{(R6)}$$
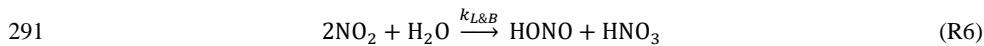
292   In this study, $k_{L\&B}$ was calculated using equation (2), with a modification of the equation:

15

293 $$k_{L\&B} = \frac{1}{8} \times v_{NO_2} \times \gamma_{g,NO_2} \times (\frac{S_{g,building}}{V} + \frac{S_{g,leaf}}{V}) \qquad \text{(Eq.2)}$$

294 $$\gamma_{g,NO_2} = 5.0 \times 10^{-7} \quad \text{(nighttime)}$$

295 $$\gamma_{g,NO_2} = 5.8 \times 10^{-6} \times (\frac{\text{light intensity}}{900}) \quad \text{(daytime)}$$

296 where γ_{g,NO_2} is the NO₂ uptake coefficient on the ground surfaces. These values are also

297 selected from sensitivity tests. Here, $\frac{S_{g,building}}{V}$ represents the ratios of the building surface

298 area to the volume, which were calculated from equation (3):

299 $$\frac{S_{g,building}}{V} = \text{PURB} \times \frac{0.3\frac{m^2}{m^3}}{100\%} \qquad \text{(Eq.3)}$$

300 where, PURB represents the percentage of building area with a maximum value of 0.3

301 (Kurtenbach et al. 2001). For vegetation areas, $\frac{S_{g,leaf}}{V}$ (the ratio of the leaf surface to volume)

302 was estimated based on leaf area index (LAI) information, along with equation (4) proposed
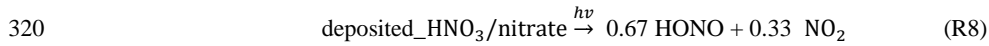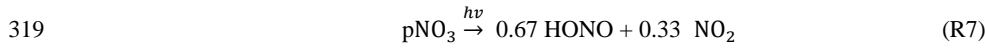
303 by Sarwar et al. (2008):

304 $$\frac{S_{g,leaf}}{V} = \frac{2 \times \text{LAI}}{H} \qquad \text{(Eq.4)}$$

305 where, H represents the height of the first layer of the model simulation (Sarwar et al., 2008;

306 Yuan et al., 2011; Zhang et al., 2012). The LAI was obtained from improved Moderate

307 Resolution Spectroradiometer (MODIS) land use data (Yuan et al., 2011).

308 **2.3.7. Photolysis reactions (RENOₓ)**

309   Several measurement studies have reported that the photolytic dissociation of

310 particulate nitrate (pNO₃) in the atmosphere (R7) may be able to explain the high HONO

311 mixing ratios observed during the daytime (Romer et al., 2018; Ye et al., 2017). Other studies

312 suggested that the photolysis reactions of HNO₃ and nitrate deposited on tree canopies and

313 artificial surfaces (R8) can also be significant sources of daytime HONO, particularly in rural

314 areas (Ye et al., 2016; Zhou et al., 2011). All these heterogeneous reactions from N(V) to N(III)

315 or N(IV) are called atmospheric 'renoxification'. Some studies have also reported that these

16

316 types of reduction reactions actually take place in the snow (Chen et al., 2019). In order to

317 better estimate the daytime mixing ratios of HONO in the atmosphere, reactions (R7) and (R8)

318 were included in the EXP8 simulation (see RENO$_x$ in Table 2).

319 $$pNO_3 \xrightarrow{hv} 0.67 \; HONO + 0.33 \; NO_2 \tag{R7}$$

320 $$deposited\_HNO_3/nitrate \xrightarrow{hv} 0.67 \; HONO + 0.33 \; NO_2 \tag{R8}$$

321 In the EXP8 simulation, we chose equations for both the photolysis rate constant of particulate

322 NO_3^- (denoted by J_{pNO_3}) and the photolysis rate constant of HNO$_3$/nitrate deposited on

323 surfaces (denoted by $J_{D\_HNO_3/nitrate}$), following the methods proposed by Zhang et al. (2022),

324 and Fu et al. (2019). These equations are presented below:

325 $$J_{pNO_3} = 118 \times J_{HNO_3} \tag{Eq.5}$$

326 $$J_{D\_HNO_3/nirate} = 48 \times J_{HNO_3} \tag{Eq.6}$$

327 where, J_{HNO_3} is the reaction rate constant of gaseous HNO$_3$ photo-dissociation, which is

328 calculated by the photolysis rate preprocessor module (JPROC) in the CMAQ model.

329 **3. Results and Discussions**

330 In this section, we first evaluated the performances of the modified CMAQ models in

331 terms of HONO mixing ratios by comparing the model outputs with ground-based observations

332 from the Olympic Park station in South Korea. We then carried out sensitivity tests to estimate

333 the contributions of the various atmospheric HONO processes to atmospheric HONO mixing

334 ratios.

335 **3.1 Observed vs Simulated HONO mixing ratios**

336 Figure 2 presents the hourly variations of the HONO mixing ratios at the Olympic Park

337 station. Observations are marked with open black circles, and colored lines represent HONO

338 mixing ratios calculated from the 8 EXP simulations. When HONO sources were added

17

339 sequentially to the experiments, the HONO mixing ratios averaged over the entire simulation

340 period increased from 0.06 ppb (EXP1 simulation) to 1.18 ppb (EXP8 simulation). The

341 averaged HONO mixing ratios in the EXP8 simulation, which took into account all the HONO

342 processes, were almost comparable to those observed from the ground (1.35 ppb of HONO).

343   The CMAQ-simulated HONO mixing ratios were particularly underestimated from 19

344 May to 23 May, 2016 (refer to gray-shadow period in Fig. 2). This period was characterized

345 by low wind speeds and poor mixing within planetary boundary layer height (PBLH), which

346 can lead to the accumulation of air pollutants (Crawford et al., 2021). On the other hand, the

347 WRF model has a strong tendency to produce higher wind speeds than the actual ones, which

348 may lead to underestimation of air pollutant concentrations (Jo et al., 2017). In particular, the

349 modeled wind speed during the stagnant period is overestimated by 36.3% compared to the

350 observed wind speed, which is significantly higher than the overestimation of 23.4% for the

351 entire KORUS-AQ period. Therefore, the underestimation of the HONO mixing ratios may be

352 caused by the overestimation of the wind speed on a given period. Despite all the discrepancies,

353 the HONO mixing ratios agree relatively well with the observed HONO mixing ratios during

354 the period of the KORUS-AQ campaign.

355
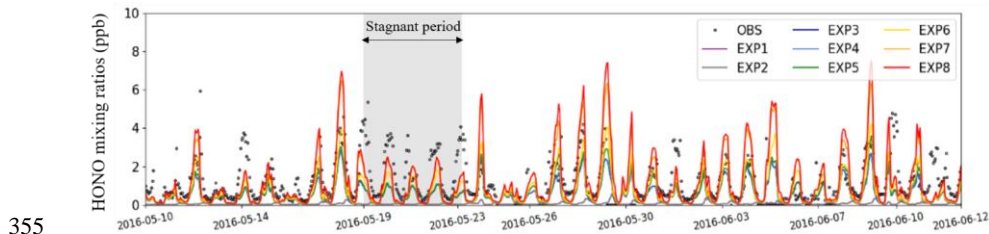
356 **Figure 2.** Hourly variations of the HONO mixing ratios (unit: ppb) at the Olympic Park station
357 in Seoul. The observations are marked with black circles and the colored lines represent the
358 HONO mixing ratios obtained from the 8 experimental simulations.

359   Figure 3 shows the diurnal variations of averaged HONO mixing ratios estimated from

360 the 8 EXP simulations, together with HONO observations at the Olympic Park station. For the

18

361 analysis of Fig. 3, daytime and nighttime are defined as 06:00–18:00 and 18:00–06:00 local

362 standard time, respectively. The EXP1 simulation showed slightly elevated HONO mixing

363 ratios during the daytime (purple line in Fig. 3) due to the net production of HONO in the gas

364 phase. The peak mixing ratio of the simulated HONO is ~0.14 ppb, which is significantly lower

365 than the observed mixing ratio. The large differences between EXP1 results and observations

366 suggest that there should be more unaccountable sources of HONO, which should be further

367 taken into account in our model simulations.

368 In the EXP2 simulation, HONO emissions from biomass burning were added. Several

369 studies have reported that direct and indirect sources emitted from biomass burning events

370 could contribute to the primary/secondary HONO formation (Jiang et al., 2023; Wang et al.,

371 2021; Gen et al., 2021). However, the addition of these biomass burning emissions resulted in

372 nearly negligible impact on the HONO mixing ratios, because no major biomass-burning

373 events occurred in South Korea during the period of the KORUS-AQ campaign (refer to Fig.

374 1b). Thus, there are minimal differences between the EXP1 and EXP2 simulations (i.e.,

375 between the purple and grey lines in Fig. 3).

376 EXP3 simulation was then carried out to examine the impact of traffic sources (TRAF)

377 on HONO mixing ratios. The average HONO mixing ratio increases to ~0.55 ppb. As

378 previously discussed in Fig. 1c, HONO emissions from traffic sources can be significant,

379 particularly in the Seoul Metropolitan Area. However, simulated levels of HONO are still much

380 lower than observed levels of HONO.

381 HONO emissions from soil (SOIL) were further included in the EXP4 simulation. As

382 discussed previously, several studies have reported that the consideration of soil emissions can

383 lead to large increases in atmospheric HONO mixing ratios, particularly in East Asia (Fig. 1e).

384 However, it was found that almost no significant changes had occurred in South Korea. This is

19

because the low soil NO_x levels in the South Korea are linked to several factors: (i) geographical feature mainly covered by forest and mountains areas; (ii) use of low nitrogen fertilizers; (iii) the reduced availability of nitrogen in the soil caused by acidic deposition; and (iv) the relatively high soil water content (SWC) over the Korean Peninsula (An et al., 2023; Kim et al., 2008).

In the EXP5 simulation, the heterogeneous reactions of NO_2 on the surfaces of atmospheric aerosols (HET_A) were further taken into account. The addition of these reactions was found to have only minor effect on the HONO mixing ratios, because γ_{a,NO_2} used in Eq. (1) is too small to enhance the HONO mixing ratios in reaction (R5). In our study, the heterogeneous reactions on the surface of atmospheric aerosols contribute only ~0.06 ppb. The heterogeneous reactions can be potentially important in more polluted regions where larger aerosol surface areas are available (Zhang et al., 2019).

On the contrary, the HONO mixing ratios can be greatly enhanced by NO_2 to HONO conversions on the surfaces of the tree leaves and buildings. These two processes were implemented in the EXP6 and EXP7 simulations (HET_L and HET_BD). In these two cases, there were significant increases in the HONO mixing ratios, particularly during the nighttime (i.e., on average, increases of 0.23 and 0.55 ppb in the HONO mixing ratios were found in the EXP6 and EXP7 simulations, respectively).

Finally, the photolytic renoxification of nitrate was added to the EXP8 simulation. In this EXP8 simulation, the averaged HONO mixing ratios increased by 0.11 ppb. The enhancement in the HONO mixing ratios was particularly large in the early morning (an increase of ~0.23 ppb was found at 6 a.m.). Overall, the EXP8 simulation produced the best HONO mixing ratios (averaged value of 1.18 ppb), compared to observed HONO mixing ratio (1.35 ppb). Also, the estimated HONO mixing ratios were more comparable than those in the

20

409 CTRL (original CMAQ v5.2.1) model simulation (represented by black squares in Fig. 3).

410 Again, it is noted that our simulations incorporated 'new HONO processes' such as: i) the

411 photo-enhanced HONO production pathway through (R5) and (R6); ii) daytime HONO

412 production from renoxification reactions through (R7) and (R8); and iii) HONO emissions

413 (refer to Table 1).

414   In addition to the graphical comparison in Fig. 3, several statistical metrics were also

415 calculated to evaluate the performances of the 8 EXP and CTRL simulations in Table 4.

416 Significant improvements were found when the HONO processes were sequentially added

417 from the EXP1 to the EXP8 simulations. For example, the index of agreement (IOA) increases

418 from 0.44 to 0.76, and the mean bias (MB) decreases drastically from -1.29 ppb to -0.17 ppb

419 from the EXP1 to the EXP8. In particular, the EXP8 simulation showed the best performance,

420 compared to the CTRL simulation during the daytime. For example, the IOA during the

421 daytime increased from 0.59 to 0.68, while the MB decreases from -0.57 to -0.34, respectively.

422 The root mean square error (RMSE) also decreased from 0.80 to 0.70 during the daytime.

423   Although the EXP8 simulation showed a notable enhancement in HONO production,

424 the HONO mixing ratios were still underestimated during the daytime. Such underestimation

425 of HONO mixing ratios during the daytime could be attributed to stronger HONO photo-

426 dissociation than in real situations. This is possibly due to failure in predicting cloud shades

427 fractions in meteorological modeling and/or due to additional sources that were not considered

428 in this study (e.g., acid displacement for HNO_3 and HCl, nitrate and Fe(II) in iron-organic

429 complex under irradiation, and renoxification of nitrate in presence of carbonaceous aerosols)

430 (Gen et al., 2021; VandenBoer et al., 2013; Wang et al., 2021). This certainly indicates that

431 additional work is needed to further investigate HONO formation and removal during the

432 daytime.

433
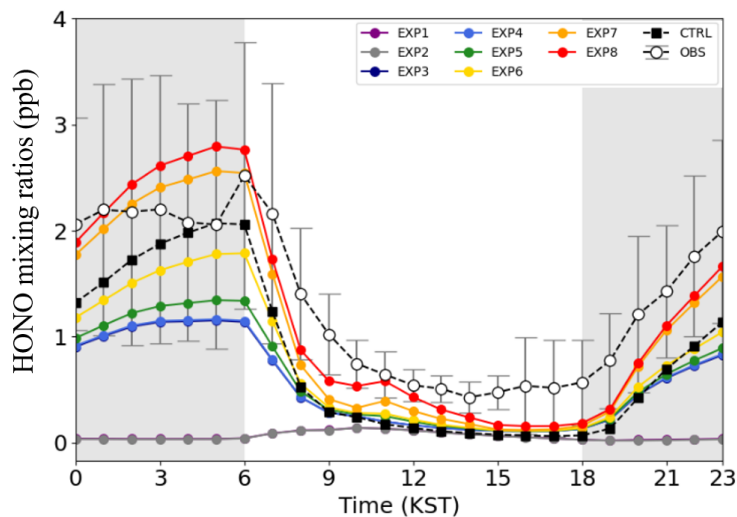
Figure 3. Diurnal variations of HONO mixing ratios (unit: ppb) at the Olympic Park station averaged over the period of the KORUS-AQ campaign. Error bars and grey-shaded areas indicate one standard deviation and nighttime (18 – 06 LST, Local Standard Time), respectively.

Table 4. Statistical analysis with modeled and observed HONO mixing ratios at the Olympic Park station, Seoul, Korea.

Experiment	Observed mean (ppb)	Modeled mean (ppb)	RMSE (ppb)	MB (ppb)	IOA
CTRL	1.35	0.78	1.06	-0.57	0.75
EXP1	1.35	0.06	1.68	-1.29	0.44
EXP2	1.35	0.06	1.68	-1.29	0.44
EXP3	1.35	0.55	1.15	-0.79	0.63
EXP4	1.35	0.56	1.15	-0.79	0.64
EXP5	1.35	0.61	1.12	-0.73	0.66
EXP6	1.35	0.75	1.02	-0.60	0.72
EXP7	1.35	1.07	1.05	-0.28	0.77
EXP8	1.35	1.18	1.12	-0.17	0.76

3.2 Relative contribution of HONO sources

22

449   Individual HONO processes affect the HONO mixing ratios in different ways. Figure

450   4 summarizes the relative contribution of HONO processes to the HONO mixing ratios. During

451   the daytime, both GAS and $RENO_x$ contribute significantly to the production of atmospheric

452   HONO molecules. In particular, the contribution of these two processes is the largest between

453   10:00 and 16:00 local time, when sunlight is strong. These two processes account for 29.1%

454   and 29.8% of the daytime HONO production, respectively, but are almost negligible during the

455   nighttime.

456   During the nighttime, TRAF (denoted by navy color in Fig. 4) contributes the large

457   portion of 47.2% of the total HONO production. However, there is a possibility that TRAF

458   might have been somewhat overestimated during the nighttime since we applied constant

459   diurnal anthropogenic NO_x emissions, including those from traffic source. In turn, HET_BD

460   and HET_L exhibit substantial contributions of 28.5% and 10.6%, respectively during the

461   nighttime. The contributions of other processes such as biomass burning (BioB) and

462   heterogeneous reactions on atmospheric aerosols (HET_A) are minimal. HET_A contributes

463   only 4.3% during the nighttime. ~~Its contribution increases to 4.2% during the daytime.~~ In terms

464   of the average 24-hour contribution, TRAF (41.4%), HET_BD (27.1%), and HET_L (11.1%)

465   are the large sources of atmospheric HONO at the Olympic Park station.

466   Using the same approach, we analyzed the HONO source contributions across South

467   Korea during the period of the KORUS-AQ campaign. As shown in Fig. 5f and 5c, HET_L

468   and TRAF were modeled to have the largest impacts on HONO production, contributing 0.15

469   ppb (41.5%) and 0.08 ppb (18.1%), respectively, across South Korea (also, refer to the

470   incremental ratio in Fig. ~~S4~~S3).

471   Fig. 6 shows the contributions of different sources to the HONO mixing ratios at 8

472   super monitoring stations. As shown in Fig. 6, each station has different characteristics in terms

473   of source contribution. In particular, the contribution of HET_L at the Daejeon is 44.4%. Also,

474   TRAF in Bulkwang, Olympic Park, Mt.Taehwa, Ulsan, and Gwangju have large contributions

475   of 41.2%, 41.4%, 29.3%, 29.6%, and 40.5%, respectively. As for TRAF and HET_BD, their

476   contributions are high only in densely populated cities (refer to Fig. 5c and 5g). On the other

477   hand, the contributions of BioB, SOIL, HET_A, and RENO$_x$ sources were insignificant, as

478   shown in Fig. 5b, 5d, 5e, and 5h.

479   Meanwhile, at the Bangnyung and Jeju stations, RENO$_x$ has the largest contribution

480   of 70.4%, and 33.2%, respectively. This is because the amounts of NO$_2$ and HONO from direct

481   emissions (BioB, TRAF, and SOIL) are relatively small. The Bangnyung and Jeju stations are

482   located on remote and less populated islands.
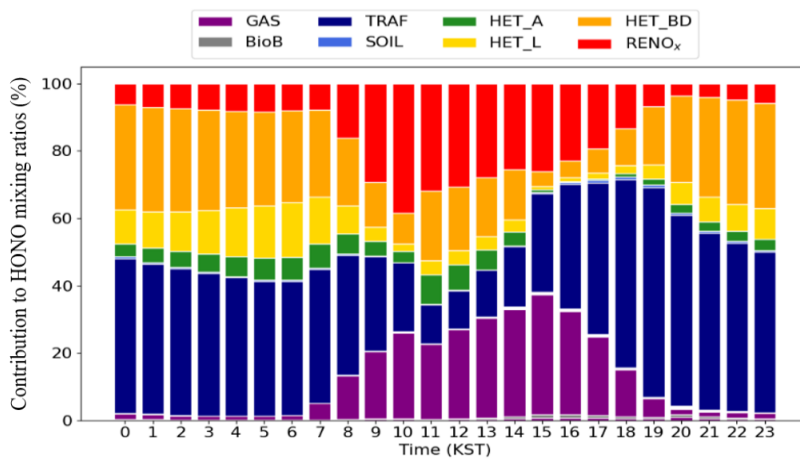
483

484   **Figure 4.** Diurnal contributions of individual HONO processes to the HONO mixing ratios at
485   the Olympic Park station during the period of the KORUS-AQ campaign.

24

486
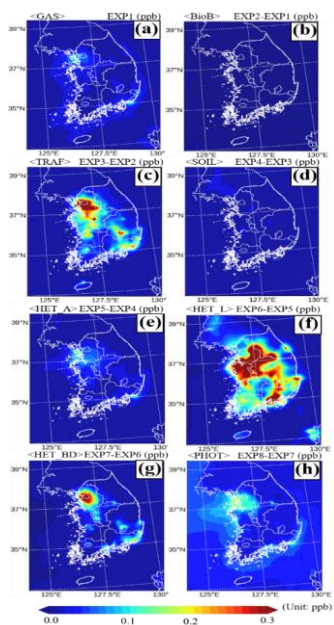
Figure 5. Spatial impacts of (a) gas phase reactions; (b) biomass burning emissions; (c) traffic emissions and (d) soil emissions; (e) heterogeneous reactions on the aerosol surfaces, (f) heterogeneous reactions on the leaf surfaces, and (g) heterogeneous reactions on the building surfaces; and (h) renoxification on HONO mixing ratios, based on model simulations during the period of the KORUS-AQ campaign in South Korea.

25
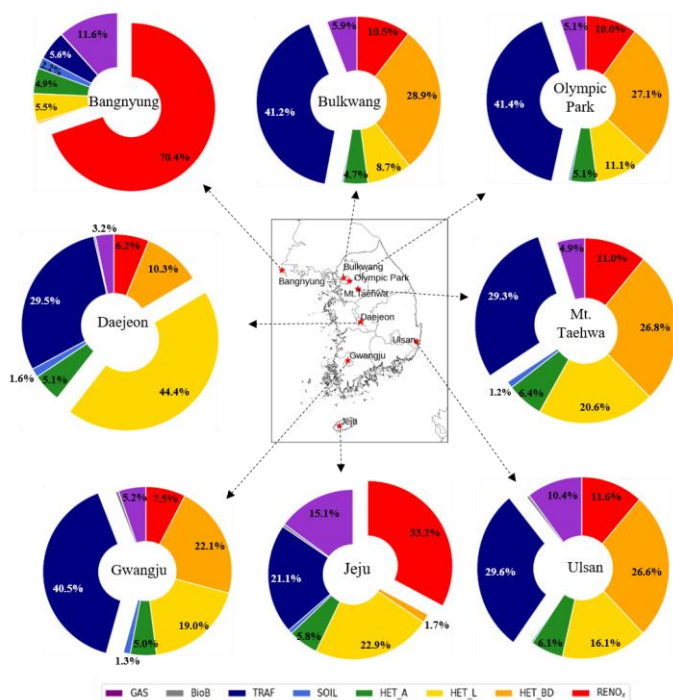
492
Figure 6. Contributions of individual processes to the average HONO mixing ratios at 8 monitoring stations during the period of the KORUS-AQ campaign.

3.3 Impact of HONO processes on atmospheric species

3.3.1 Impact on atmospheric species

We also investigated the effect of HONO processes on atmospheric levels of HO_x (=$OH + HO_2$), HCHO, O_3, NO, and $PM_{2.5}$ at the Olympic Park station. Figure 7 presents the diurnal concentrations of these gaseous and particulate species at the Olympic Park station. The mixing ratios of OH and HO_2 radicals in the EXP8 simulation increased by 0.02 ppt (35.2%) and 0.23 ppt (39.2%), respectively, compared to those in the CTRL simulation. This is certainly due to the enhancement in OH levels due to HONO photo-dissociation, and then HO_2 levels in the HO_x cycle. As shown in Fig. 7a (and 7b), the OH (and HO_2) mixing ratios increased from 0.21 ppt to 0.29 ppt (1.71 ppt to 2.28 ppt) at 1 p.m. local standard time. Subsequently, the

26

505 HCHO mixing ratios were also enhanced by 0.18 ppb (8.8%), due to increased VOC oxidation

506 resulting from elevated levels of OH radicals (Fig. 7c). On the contrary, the NO mixing ratios

507 in the EXP8 simulation decreased by 2.13 ppb (20.1%). This may be due to an increase in the

508 mixing ratios of HO_2 and RO_2 radicals (organic peroxyl radicals) reacting with NO molecules

509 (Fig. 7d). In other words, the reduced levels of NO indicate active NO to NO_2 conversion via

510 $NO+HO_2$ and $NO+RO_2$ reactions. Such active NO to NO_2 conversion increases the mixing

511 ratio of atmospheric ozone because these two reactions are rate-determining reactions for ozone

512 production. This is presented in Fig. 7e. In Fig. 7e, the modeled ozone mixing ratios increased,

513 approaching the observed ozone mixing ratios. This is another good result showing that the

514 incorporation of atmospheric HONO processes may be able to enhance the accuracy of

515 prediction of ozone mixing ratios. More details about ozone production are discussed in Sect.

516 3.3.2.

517 Elevated levels of atmospheric O_3 and HO_x can change the rates of particulate nitrate

518 and sulfate production. In particular, the formation of particulate nitrates and sulfates can also

519 be enhanced by increasing the levels of HNO_3, N_2O_5, and H_2SO_4. In addition, the nitrate

520 concentration can also be enhanced by the HONO reaction (i.e., via $NO_2 + H_2O \rightarrow H^+ + NO_3^-$

521 + HONO, as accounted for by ~~R5~~R6) during the nighttime. In total, the addition of HONO

522 processes increases $PM_{2.5}$ by 4.19 $\mu g\ m^{-3}$ (18.6%) at the Olympic Park station. However, $PM_{2.5}$

523 in the EXP8 simulation was still underestimated by 3.16 $\mu g\ m^{-3}$ at the Olympic Park station, as

524 shown in Fig. 7f. There are several potential reasons for this underestimation, such as the

525 underestimation of secondary organic aerosol (SOA) formation (e.g., Murphy et al., 2017).

526 This issue may require further investigation in the future.

527 Figure S~~4~~3 presents similar results for 320 AIR KOREA monitoring stations in South

528 Korea. The impacts of HONO processes on atmospheric levels of OH, HO_2, O_3, and $PM_{2.5}$ are

529 also presented in Fig. S~~5~~4. Overall, we found that incorporating HONO chemistry into the

530   modeling system tends to enhance the mixing ratios of HO_x, which in turn increases the mixing

531   ratios of O_3 and $PM_{2.5}$.

532
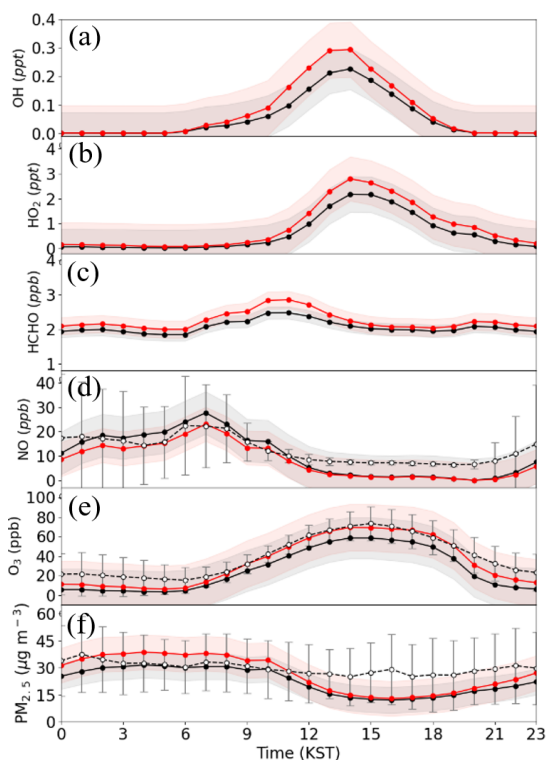
Figure 7. Diurnal variations of the mixing ratios of (a) OH, (b) HO_2, (c) HCHO, (d) NO, (e) O_3, and (f) $PM_{2.5}$ (black lines represent the mixing ratios from the CTRL simulation and the red lines represent those from the EXP8 simulation) and observations (marked with white open cycles) at the Olympic Park station during the period of the KORUS-AQ campaign. Shaded areas represent one standard deviation for each simulation.

3.3.2 Impact on net ozone production

539   The ozone mixing ratio is determined by the balance between ozone formation and

540   destruction in the atmosphere. To better understand the impacts of HONO chemistry on ozone

541   production, we quantitatively analyze the rate of net ozone production ($P(O_3)$). The $P(O_3)$ is

542   defined by equation (7):

28

543     $$P(O_3) = F(O_3) - D(O_3) \qquad \text{(Eq. 7)}$$

544   where, $F(O_3)$ and $D(O_3)$ represent the rate of ozone formation and destruction, respectively.

545     $F(O_3)$ and $D(O_3)$ can be calculated from equations (8) and (9), respectively (Mazzuca et al.,

546   2016; Song et al., 2003).

547     $$F(O_3) = k_{HO_2+NO}[HO_2][NO] + k_{RO_2+NO}[RO_2][NO] \qquad \text{(Eq. 8)}$$

548 $$D(O_3) = k_{NO_2+OH}[NO_2][OH] + k_{O_3+VOC}[O_3][VOC] + k_{O(1D)+H_2O}[O(^1D)][H_2O]$$

549     $$+ k_{O_3+OH}[O_3][OH] + k_{O_3+HO_2}[O_3][HO_2] + k_{RO_2+NO_2}[RO_2][NO_2]$$

550     $$+ 2k_{NO_3+VOC}[NO_3][VOC] + 3k_{het}[N_2O_5] \qquad \text{(Eq. 9)}$$

551   where k_i represents the reaction rate constants for each reaction i. In particular, k_{het} denotes the

552   heterogeneous reaction rate constants of N_2O_5 radicals.

553   Figure 8a shows the diurnal variations of $F(O_3)$, $D(O_3)$, and $P(O_3)$ from the CTRL and

554   EXP8 simulations. Including HONO processes in the EXP8 simulation resulted in an average

555     $P(O_3)$ that was 10.6% higher than in the CTRL simulation. This is the primary reason for the

556   ozone enhancement in Fig. 7e.

557   Figures 8b and 8c provide more details about the budget of ozone production. The

558   main increase in $F(O_3)$ occurred through the reactions of $HO_2 + NO$ and $RO_2 + NO$. On the

559   other hand, the increase in $D(O_3)$ was mainly controlled by the $NO_2 + OH$ reaction at the

560   Olympic Park station. The increases in the $HO_2 + NO$ and $RO_2 + NO$ reaction rate exceeded

561   the increases in the reaction rate of $NO_2 + OH$, leading to the net positive ozone production

562   (i.e., positive $P(O_3)$) shown in Fig. 8a.

29
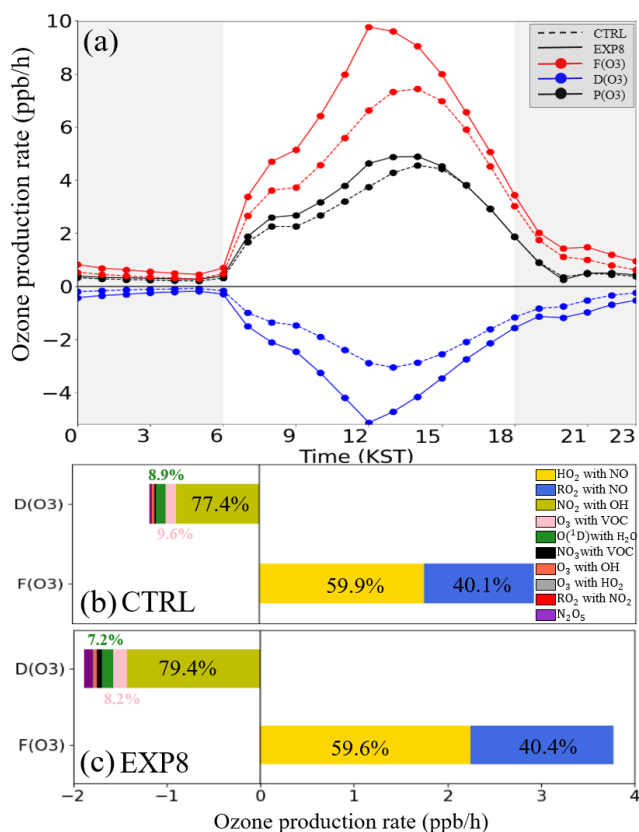
Figure 8. Diurnal variations of (a) net ozone production rate (P(O₃); black line), ozone formation rate (F(O₃); red line), and ozone loss rate (D(O₃); blue line). The dashed and solid lines represent the CTRL and EXP8 simulations, respectively. Cumulative bar chart for D(O₃) and F(O₃) in case of (b) CTRL and (c) EXP8 simulations at the Olympic Park station during the period of the KORUS-AQ campaign.

4. Conclusions

In this study, we successfully incorporated the following HONO processes into the CMAQ modeling framework to enhance the accuracy in the predictions of HONO mixing ratios: i) gas-phase HONO reactions; ii) HONO emission from biomass burning; iii) HONO emission from traffic and soil; iv) photo-induced heterogeneous reactions on the surfaces of atmospheric aerosols, tree leaves, and buildings; and v) photolysis reactions of particulate

575   nitrate and deposited HNO_3/nitrate. The analysis showed that the incorporation of HONO

576   processes into the CMAQ model framework increased the average HONO mixing ratios from

577   0.78 ppb to 1.18 ppb compared to the CTRL simulation. Average mixing ratios of HONO and

578   its diurnal patterns became much more comparable to observations, with large improvements

579   in statistical parameters. Especially during the daytime, IOA increased from 0.59 to 0.68, while

580   the MB decreased from -0.57 ppb to -0.34 ppb, and RMSE dropped from 0.80 ppb to 0.70 ppb,

581   as HONO processes were fully incorporated into the CMAQ model.

582   Several findings also emerged from the sensitivity simulations. First, each HONO process

583   had a different effect on the HONO mixing ratios during the daytime and the nighttime at the

584   Olympic Park station. For example, the GAS (29.1%) and $RENO_x$ processes (29.8%) had major

585   contributions to the mixing ratios of HONO during the daytime, while the TRAF (47.2%) and

586   HET_BD (28.5%) processes had large contributions to the mixing ratios of HONO during the

587   nighttime. During the period of the KORUS-AQ campaign, HONO mixing ratios estimated at

588   the Olympic Park station were enhanced by an average of 41.4% (TRAF), 27.1% (HET_BD),

589   and 11.1% (HET_L).

590   In the experimental simulation including all the HONO processes (i.e., EXP8 simulation),

591   the mixing ratios of OH, HO_2, HCHO, O_3, and $PM_{2.5}$ at the Olympic Park station increased by

592   0.02 ppt (35.2%), 0.23 ppt (39.2%), 0.18 ppb (8.8%), 7.86 ppb (30.8%), and 4.19 μg m^{-3}

593   (18.6%), respectively, compared to those from the CTRL simulation. The net ozone production

594   rate was enhanced by 0.19 ppb h^{-1} (10.6%) with the EXP8 simulation. This increases in $P(O_3)$

595   were caused mainly by the increased reaction rates of $HO_2 + NO$.

596   In this study, we improved our understanding of atmospheric HONO processes in

597   South Korea. Nevertheless, we believe that both further field studies and modeling

598   investigations are necessary for many remaining HONO-related issues such as NO_2 uptake

31

599 coefficient, possible missing HONO sources, and daytime photochemical reaction pathways of

600 HONO. Such studies will also help to further improve the performances of current CTMs.

601 For example, the Airborne and Satellite Investigation of Asian Air Quality (ASIA-AQ)

602 field campaign organized by the National Institute of Environmental Research (NIER) in Korea

603 and the National Aeronautics and Space Administration (NASA) in the U.S. is planned in 2024

604 in South Korea. In this campaign, the HONO mixing ratios are scheduled to be measured in

605 the aircraft and at the ground station. This joint campaign is thus expected to provide a valuable

606 opportunity to expand our knowledge on atmospheric HONO processes and HONO photo-

607 chemistry.

608

Code and data availability

610 After user registration, the WRF model 3.8.1 (https://www2.mmm.ucar.edu/wrf/users, last access: 11
611 April 2024) and CMAQ v5.2.1 (https://doi.org/10.5281/zenodo.1212601, last access: 11 April 2024)
612 are available from web page. The observation data we used can be accessed at https://www-
613 air.larc.nasa.gov/cgi-bin/ArcView/korusaq?GROUND-NIER-OLYMPIC-PARK=1 (last access: 11
614 April 2024).

615

Author contribution

617 **KYK** designed experiments and led manuscript writing and conceptualization. **KMH** and **CHS**
618 supervised this project and contributed to experimental design and manuscript writing. **HJL, RB,**
619 **JHY, GY,** and **BYK** performed research development. **JM** contributed to editing and writing review.
620 **JHW** and **SJC** provided useful datasets.

621

Competing interests

623 Chul H. Song is a member of the editorial board of *Atmospheric Chemistry and Physics*. The authors
624 declare that they have no conflict of interest.

625

Acknowledgement

632

References

Acker, K., Möller, D., Wieprecht, W., Meixner, F. X., Bohn, B., Gilge, S., Plass-Dülmer, C., and Berresheim, H.: Strong daytime production of OH from HNO2 at a rural mountain site, Geophysical Research Letters, 33, https://doi.org/10.1029/2005GL024643, 2006.

Alicke, B., Geyer, A., Hofzumahaus, A., Holland, F., Konrad, S., Pätz, H., Schäfer, J., Stutz, J., Volz-Thomas, A., and Platt, U.: OH formation by HONO photolysis during the BERLIOZ experiment, Journal of Geophysical Research: Atmospheres, 108, PHO 3-1-PHO 3-17, https://doi.org/10.1029/2001JD000579, 2003.

An, J., Li, Y., Chen, Y., Li, J., Qu, Y., and Tang, Y.: Enhancements of major aerosol components due to additional HONO sources in the North China Plain and implications for visibility and haze, Advances in Atmospheric Sciences, 30, 57-66, https://doi.org/10.1007/s00376-012-2016-9, 2013.

An, Y., Shim, W., and Jeong, G.: High-Resolution Digital Soil Maps of Forest Soil Nitrogen across South Korea Using Three Machine Learning Algorithms, Forests, 14, 1141, https://doi.org/10.3390/f14061141, 2023.

Appel, K. W., Napelenok, S., Hogrefe, C., Pouliot, G., Foley, K. M., Roselle, S. J., Pleim, J. E., Bash, J., Pye, H. O., and Heath, N.: Overview and evaluation of the Community Multiscale Air Quality (CMAQ) modeling system version 5.2, International Technical Meeting on Air Pollution Modelling and its Application, 69-73, https://doi.org/10.1007/978-3-319-57645-9_11

Bejan, I., Abd El Aal, Y., Barnes, I., Benter, T., Bohn, B., Wiesen, P., and Kleffmann, J.: The photolysis of ortho-nitrophenols: a new gas phase source of HONO, Physical Chemistry Chemical Physics, 8, 2028-2035, https://doi.org/10.1039/B516590C, 2006.

Binkowski, F. S. and Roselle, S. J.: Models-3 Community Multiscale Air Quality (CMAQ) model aerosol component 1. Model description, Journal of geophysical research: Atmospheres, 108, https://doi.org/10.1029/2001JD001409, 2003.

Burkholder, J., Sander, S., Abbatt, J., Barker, J., Huie, R., Kolb, C., Kurylo, M., Orkin, V., Wilmouth, D., and Wine, P.: Chemical kinetics and photochemical data for use in atmospheric studies, evaluation no. 18, JPL publication 15-10; Jet Propulsion Laboratory, Pasadena, CA, Pasadena, http://jpldataeval.jpl.nasa.gov, 2015.

Byun, D. and Schere, K. L.: Review of the governing equations, computational algorithms, and other components of the Models-3 Community Multiscale Air Quality (CMAQ) modeling system, 2006.

Carter, W. P.: Development of the SAPRC-07 chemical mechanism, Atmospheric Environment, 44, 5324-5335, https://doi.org/10.1016/j.atmosenv.2010.01.026, 2010.

Chen, F. and Dudhia, J.: Coupling an advanced land surface–hydrology model with the Penn State–NCAR MM5 modeling system. Part I: Model implementation and sensitivity, Monthly weather review, 129, 569-585, https://doi.org/10.1175/1520-0493(2001)129<0569:CAALSH>2.0.CO;2, 2001.

Chen, Q., Edebeli, J., McNamara, S. M., Kulju, K. D., May, N. W., Bertman, S. B., Thanekar, S., Fuentes, J. D., and Pratt, K. A.: HONO, Particulate Nitrite, and Snow Nitrite at a Midlatitude Urban Site during Wintertime, ACS Earth and Space Chemistry, 3, 811-822, https://doi.org/10.1021/acsearthspacechem.9b00023, 2019.

Cheng, Z., Wang, S., Fu, X., Watson, J. G., Jiang, J., Fu, Q., Chen, C., Xu, B., Yu, J., and Chow, J. C.: Impact of biomass burning on haze pollution in the Yangtze River delta, China: a case study in summer 2011, Atmospheric Chemistry and Physics, 14, 4573-4585, https://doi.org/10.5194/acp-14-4573-2014, 2014.

Colussi, A. J., Enami, S., Yabushita, A., Hoffmann, M. R., Liu, W.-G., Mishra, H., and Goddard III, W. A.: Tropospheric aerosol as a reactive intermediate, Faraday Discussions, 165, 407-420, https://doi.org/10.1039/C3FD00040K, 2013.

Crawford, J. H., Ahn, J.-Y., Al-Saadi, J., Chang, L., Emmons, L. K., Kim, J., Lee, G., Park, J.-H., Park, R. J., Woo, J. H., Song, C.-K., Hong, J.-H., Hong, Y.-D., Lefer, B. L., Lee, M., Lee, T., Kim, S., Min, K.-E., Yum, S. S., Shin, H. J., Kim, Y.-W., Choi, J.-S., Park, J.-S., Szykman, J. J., Long, R. W., Jordan, C. E., Simpson, I. J., Fried, A., Dibb, J. E., Cho, S., and Kim, Y. P.: The Korea–United States Air Quality (KORUS-AQ) field study, Elementa, 9, 00163, https://doi.org/10.1525/elementa.2020.00163, 2021.

Crutzen, P. J. and Andreae, M. O.: Biomass burning in the tropics: Impact on atmospheric chemistry and biogeochemical cycles, Science, 250, 1669-1678, DOI: 10.1126/science.250.4988.1669, 1990.

33

681 Czader, B., Rappenglück, B., Percell, P., Byun, D., Ngan, F., and Kim, S.: Modeling nitrous acid and its impact
682   on ozone and hydroxyl radical during the Texas Air Quality Study 2006, Atmospheric Chemistry & Physics
683   Discussions, 12, https://doi.org/10.5194/acp-12-6939-2012,2012.
684 Czader, B. H., Choi, Y., Li, X., Alvarez, S., and Lefer, B.: Impact of updated traffic emissions on HONO mixing
685   ratios simulated for urban site in Houston, Texas, Atmospheric Chemistry and Physics, 15, 1253,
686   https://doi.org/10.5194/acp-15-1253-2015, 2015.
687 Foley, K., Roselle, S., Appel, K., Bhave, P., Pleim, J., Otte, T., Mathur, R., Sarwar, G., Young, J., and Gilliam, R.:
688   Incremental testing of the Community Multiscale Air Quality (CMAQ) modeling system version 4.7,
689   Geoscientific Model Development, 3, 205, https://doi.org/10.5194/gmd-3-205-2010, 2010.
690 Fu, X., Wang, T., Zhang, L., Li, Q., Wang, Z., Xia, M., Yun, H., Wang, W., Yu, C., Yue, D., Zhou, Y., Zheng, J.,
691   and Han, R.: The significant contribution of HONO to secondary pollutants during a severe winter pollution
692   event in southern China, Atmos. Chem. Phys., 19, 1–14, https://doi.org/10.5194/acp-19-1-2019, 2019.
693 Gen, M., Zhang, R., and Chan, C. K.: Nitrite/nitrous acid generation from the reaction of nitrate and Fe (II)
694   Promoted by photolysis of iron–organic complexes, Environmental Science & Technology, 55, 15715-15723,
695   https://doi.org/10.1021/acs.est.1c05641, 2021.
696 Gligorovski, S.: Nitrous acid (HONO): An emerging indoor pollutant, Journal of Photochemistry and
697   Photobiology A: Chemistry, 314, 1-5, https://doi.org/10.1016/j.jphotochem.2015.06.008, 2016.
698 Grell, G. A. and Freitas, S. R.: A scale and aerosol aware stochastic convective parameterization for weather and
699   air quality modeling, Atmos. Chem. Phys, 14, 5233-5250, https://doi.org/10.5194/acp-14-5233-2014, 2014.
700 Guenther, A. B., Jiang, X., Heald, C. L., Sakulyanontvittaya, T., Duhl, T., Emmons, L. K., and Wang, X.: The
701   Model of Emissions of Gases and Aerosols from Nature version 2.1 (MEGAN2.1): an extended and updated
702   framework for modeling biogenic emissions, Geosci. Model Dev., 5, 1471–1492, https://doi.org/10.5194/gmd-
703   5-1471-2012, 2012.
704 Gutzwiller, L., Arens, F., Baltensperger, U., Gäggeler, H. W., and Ammann, M.: Significance of semivolatile diesel
705   exhaust organics for secondary HONO formation, Environmental science & technology, 36, 677-682,
706   https://doi.org/10.1021/es015673b, 2002.
707 Han, C., Yang, W., Yang, H., and Xue, X.: Enhanced photochemical conversion of NO2 to HONO on humic acids
708   in the presence of benzophenone, Environmental Pollution, 231, 979-986,
709   https://doi.org/10.1016/j.envpol.2017.08.107, 2017.
710 Hao, Q., Jiang, N., Zhang, R., Yang, L., and Li, S.: Characteristics, sources, and reactions of nitrous acid during
711   winter at an urban site in the Central Plains Economic Region in China, Atmospheric Chemistry and Physics,
712   20, 7087-7102, https://doi.org/10.5194/acp-20-7087-2020, 2020.
713 Harris, G. W., Carter, W. P., Winer, A. M., Pitts, J. N., Platt, U., and Perner, D.: Observations of nitrous acid in the
714   Los Angeles atmosphere and implications for predictions of ozone-precursor relationships, Environmental
715   science & technology, 16, 414-419, https://doi.org/10.1021/es00101a009, 1982.
716 Hendrick, F., Müller, J.-F., Clémer, K., Wang, P., De Mazière, M., Fayt, C., Gielen, C., Hermans, C., Ma, J. Z.,
717   Pinardi, G., Stavrakou, T., Vlemmix, T., and Van Roozendael, M.: Four years of ground-based MAX-DOAS
718   observations of HONO and NO$_2$ in the Beijing area, Atmos. Chem. Phys., 14, 765–781,
719   https://doi.org/10.5194/acp-14-765-2014, 2014.
720 Hong, S.-Y. and Lim, J.-O. J.: The WRF single-moment 6-class microphysics scheme (WSM6), Asia-Pacific
721   Journal of Atmospheric Sciences, 42, 129-151, 2006.
722 Hong, S.-Y., Noh, Y., and Dudhia, J.: A new vertical diffusion package with an explicit treatment of entrainment
723   processes, Monthly weather review, 134, 2318-2341, https://doi.org/10.1175/MWR3199.1, 2006.
724 Hou, S., Tong, S., Ge, M., and An, J.: Comparison of atmospheric nitrous acid during severe haze and clean
725   periods in Beijing, China, Atmospheric environment, 124, 199-206,
726   https://doi.org/10.1016/j.atmosenv.2015.06.023, 2016.
727 Hutzell, W., Luecken, D., Appel, K., and Carter, W.: Interpreting predictions from the SAPRC07 mechanism based
728   on regional and continental simulations, Atmospheric Environment, 46, 417-429,
729   https://doi.org/10.1016/j.atmosenv.2011.09.030, 2012.

Iacono, M. J., Delamere, J. S., Mlawer, E. J., Shephard, M. W., Clough, S. A., and Collins, W. D.: Radiative forcing by long-lived greenhouse gases: Calculations with the AER radiative transfer models, Journal of Geophysical Research: Atmospheres, 113, https://doi.org/10.1029/2008JD009944, 2008.

Jia, C., Tong, S., Zhang, W., Zhang, X., Li, W., Wang, Z., Wang, L., Liu, Z., Hu, B., and Zhao, P.: Pollution characteristics and potential sources of nitrous acid (HONO) in early autumn 2018 of Beijing, Science of The Total Environment, 735, 139317, https://doi.org/10.1016/j.scitotenv.2020.139317, 2020.

Jiang, H., Bao, F., Wang, J., Chen, J., Zhu, Y., Huang, D., Chen, C., and Zhao, J.: Direct formation of electronic excited NO2 contributes to the high yield of HONO during photosensitized renoxification, Environmental Science & Technology, 57, 11144-11151, https://doi.org/10.1021/acs.est.3c01342, 2023.

Jiménez, P. A., Dudhia, J., González-Rouco, J. F., Navarro, J., Montávez, J. P., and García-Bustamante, E.: A revised scheme for the WRF surface layer formulation, Monthly Weather Review, 140, 898-918, https://doi.org/10.1175/MWR-D-11-00056.1, 2012.

Jo, Y. J., Lee, H. J., Chang, L. S., and Kim, C. H.: Sensitivity study of the initial meteorological fields on the PM10 concentration predictions using CMAQ modeling, J. Korean Soc. Atmos. Environ., 33, 554–569, https://doi.org/10.5572/kosae.2017.33.6.554, 2017.

Karamchandani, P., Emery, C., Yarwood, G., Lefer, B., Stutz, J., Couzo, E., and Vizuete, W.: Implementation and refinement of a surface model for heterogeneous HONO formation in a 3-D chemical transport model, Atmospheric Environment, 112, 356-368, https://doi.org/10.1016/j.atmosenv.2015.01.046, 2015.

Keywood, M., Selleck, P., Reisen, F., Cohen, D., Chambers, S., Cheng, M., Cope, M., Crumeyrolle, S., Dunne, E., Emmerson, K., Fedele, R., Galbally, I., Gillett, R., Griffiths, A., Guerette, E.-A., Harnwell, J., Humphries, R., Lawson, S., Miljevic, B., Molloy, S., Powell, J., Simmons, J., Ristovski, Z., and Ward, J.: Comprehensive aerosol and gas data set from the Sydney Particle Study, Earth Syst. Sci. Data, 11, 1883–1903, https://doi.org/10.5194/essd-11-1883-2019, 2019.

Kim, C.-H., Park, I.-S., Kim, S.-K., Son, H.-Y., Lee, J.-J., Lee, J.-B., Song, C.-K., and Shim, J.-M.: Estimation and mapping of nitrogen uptake by forest in South Korea, Water, air, and soil pollution, 187, 315-325, https://doi.org/10.1007/s11270-007-9519-5, 2008.

Kim, S., VandenBoer, T. C., Young, C. J., Riedel, T. P., Thornton, J. A., Swarthout, B., Sive, B., Lerner, B., Gilman, J. B., and Warneke, C.: The primary and recycling sources of OH during the NACHTT-2011 campaign: HONO as an important OH primary source in the wintertime, Journal of Geophysical Research: Atmospheres, 119, 6886-6896, https://doi.org/10.1002/2013JD019784, 2014.

Kirchstetter, T. W., Harley, R. A., and Littlejohn, D.: Measurement of nitrous acid in motor vehicle exhaust, Environmental science & technology, 30, 2843-2849, https://doi.org/10.1021/es960135y, 1996.

Kleffmann, J., Gavriloaiei, T., Hofzumahaus, A., Holland, F., Koppmann, R., Rupp, L., Schlosser, E., Siese, M., and Wahner, A.: Daytime formation of nitrous acid: A major source of OH radicals in a forest, Geophysical Research Letters, 32, https://doi.org/10.1029/2005GL022524, 2005.

Kurtenbach, R., Becker, K., Gomes, J., Kleffmann, J., Lörzer, J., Spittler, M., Wiesen, P., Ackermann, R., Geyer, A., and Platt, U.: Investigations of emissions and heterogeneous formation of HONO in a road traffic tunnel, Atmospheric Environment, 35, 3385-3394, https://doi.org/10.1016/S1352-2310(01)00138-8, 2001.

Lee, J. D., Whalley, L. K., Heard, D. E., Stone, D., Dunmore, R. E., Hamilton, J. F., Young, D. E., Allan, J. D., Laufs, S., and Kleffmann, J.: Detailed budget analysis of HONO in central London reveals a missing daytime source, Atmos. Chem. Phys., 16, 2747–2764, https://doi.org/10.5194/acp-16-2747-2016, 2016.

Levy, M., Zhang, R., Zheng, J., Zhang, A. L., Xu, W., Gomez-Hernandez, M., Wang, Y., and Olaguer, E.: Measurements of nitrous acid (HONO) using ion drift-chemical ionization mass spectrometry during the 2009 SHARP field campaign, Atmospheric Environment, 94, 231-240, https://doi.org/10.1016/j.atmosenv.2014.05.024, 2014.

Li, D., Xue, L., Wen, L., Wang, X., Chen, T., Mellouki, A., Chen, J., and Wang, W.: Characteristics and sources of nitrous acid in an urban atmosphere of northern China: Results from 1-yr continuous observations, Atmospheric Environment, 182, 296-306, https://doi.org/10.1016/j.atmosenv.2018.03.033, 2018.

Li, G., Lei, W., Zavala, M., Volkamer, R., Dusanter, S., Stevens, P., and Molina, L. T.: Impacts of HONO sources on the photochemistry in Mexico City during the MCMA-2006/MILAGO Campaign, Atmos. Chem. Phys., 10, 6551–6567, https://doi.org/10.5194/acp-10-6551-2010, 2010.

Li, X., Brauers, T., Häseler, R., Bohn, B., Fuchs, H., Hofzumahaus, A., Holland, F., Lou, S., Lu, K. D., Rohrer, F., Hu, M., Zeng, L. M., Zhang, Y. H., Garland, R. M., Su, H., Nowak, A., Wiedensohler, A., Takegawa, N., Shao, M., and Wahner, A.: Exploring the atmospheric chemistry of nitrous acid (HONO) at a rural site in Southern China, Atmos. Chem. Phys., 12, 1497–1513, https://doi.org/10.5194/acp-12-1497-2012, 2012.

Li, X., Rohrer, F., Hofzumahaus, A., Brauers, T., Häseler, R., Bohn, B., Broch, S., Fuchs, H., Gomm, S., and Holland, F.: Missing gas-phase source of HONO inferred from Zeppelin measurements in the troposphere, Science, 344, 292-296, https://doi.org/10.1126/science.1248999 2014.

Lu, X., Wang, Y., Li, J., Shen, L., and Fung, J. C.: Evidence of heterogeneous HONO formation from aerosols and the regional photochemical impact of this HONO source, Environmental Research Letters, 13, 114002, https://doi.org/10.1088/1748-9326/aae492, 2018.

Mazzuca, G. M., Ren, X., Loughner, C. P., Estes, M., Crawford, J. H., Pickering, K. E., Weinheimer, A. J., and Dickerson, R. R.: Ozone production and its sensitivity to NO_x and VOCs: results from the DISCOVER-AQ field experiment, Houston 2013, Atmos. Chem. Phys., 16, 14463–14474, https://doi.org/10.5194/acp-16-14463-2016, 2016.

Meusel, H., Kuhn, U., Reiffs, A., Mallik, C., Harder, H., Martinez, M., Schuladen, J., Bohn, B., Parchatka, U., Crowley, J. N., Fischer, H., Tomsche, L., Novelli, A., Hoffmann, T., Janssen, R. H. H., Hartogensis, O., Pikridas, M., Vrekoussis, M., Bourtsoukidis, E., Weber, B., Lelieveld, J., Williams, J., Pöschl, U., Cheng, Y., and Su, H.: Daytime formation of nitrous acid at a coastal remote site in Cyprus indicating a common ground source of atmospheric HONO and NO, Atmos. Chem. Phys., 16, 14475–14493, https://doi.org/10.5194/acp-16-14475-2016, 2016.

Meusel, H., Tamm, A., Kuhn, U., Wu, D., Leifke, A. L., Fiedler, S., Ruckteschler, N., Yordanova, P., Lang-Yona, N., Pöhlker, M., Lelieveld, J., Hoffmann, T., Pöschl, U., Su, H., Weber, B., and Cheng, Y.: Emission of nitrous acid from soil and biological soil crusts represents an important source of HONO in the remote atmosphere in Cyprus, Atmos. Chem. Phys., 18, 799–813, https://doi.org/10.5194/acp-18-799-2018, 2018.

Monks, P. S., Granier, C., Fuzzi, S., Stohl, A., Williams, M. L., Akimoto, H., Amann, M., Baklanov, A., Baltensperger, U., and Bey, I.: Atmospheric composition change–global and regional air quality, Atmospheric environment, 43, 5268-5350, https://doi.org/10.1016/j.atmosenv.2009.08.021, 2009.

Murphy, B. N., Woody, M. C., Jimenez, J. L., Carlton, A. M. G., Hayes, P. L., Liu, S., Ng, N. L., Russell, L. M., Setyan, A., Xu, L., Young, J., Zaveri, R. A., Zhang, Q., and Pye, H. O. T.: Semivolatile POA and parameterized total combustion SOA in CMAQv5.2: impacts on source strength and partitioning, Atmos. Chem. Phys., 17, 11107–11133, https://doi.org/10.5194/acp-17-11107-2017, 2017.

Nagai, K. and Kubota, M.: On the volatilization of nitrogen during nitrification in soils under vinyl covered culture. 5. on the effects of iron complex salts and treatments with nitrates or chloride on volatilization of nitrous acid, Jap J Sci Soil and Manure, 1972.

Nakashima, Y. and Kajii, Y.: Determination of nitrous acid emission factors from a gasoline vehicle using a chassis dynamometer combined with incoherent broadband cavity-enhanced absorption spectroscopy, Science of The Total Environment, 575, 287-293, https://doi.org/10.1016/j.scitotenv.2016.10.050, 2017.

Nie, W., Ding, A. J., Xie, Y. N., Xu, Z., Mao, H., Kerminen, V.-M., Zheng, L. F., Qi, X. M., Huang, X., Yang, X.-Q., Sun, J. N., Herrmann, E., Petäjä, T., Kulmala, M., and Fu, C. B.: Influence of biomass burning plumes on HONO chemistry in eastern China, Atmos. Chem. Phys., 15, 1147–1159, https://doi.org/10.5194/acp-15-1147-2015, 2015.

Oswald, R., Behrendt, T., Ermel, M., Wu, D., Su, H., Cheng, Y., Breuninger, C., Moravek, A., Mougin, E., and Delon, C.: HONO emissions from soil bacteria as a major source of atmospheric reactive nitrogen, Science, 341, 1233-1235, https://doi.org/10.1126/science.1242266, 2013.

Pathak, R. K., Wu, W. S., and Wang, T.: Summertime $PM_{2.5}$ ionic species in four major cities of China: nitrate formation in an ammonia-deficient atmosphere, Atmos. Chem. Phys., 9, 1711–1722, https://doi.org/10.5194/acp-9-1711-2009, 2009.

Rappenglück, B., Lubertino, G., Alvarez, S., Golovko, J., Czader, B., and Ackermann, L.: Radical precursors and related species from traffic as observed and modeled at an urban highway junction, Journal of the Air & Waste Management Association, 63, 1270-1286, https://doi.org/10.1080/10962247.2013.822438, 2013.

Reisinger, A. R.: Observations of HNO2 in the polluted winter atmosphere: possible heterogeneous production on aerosols, Atmospheric Environment, 34, 3865-3874, https://doi.org/10.1016/S1352-2310(00)00179-5, 2000.

Ren, X., Harder, H., Martinez, M., Lesher, R. L., Oliger, A., Simpas, J. B., Brune, W. H., Schwab, J. J., Demerjian, K. L., and He, Y.: OH and HO2 chemistry in the urban atmosphere of New York City, Atmospheric Environment, 37, 3639-3651, https://doi.org/10.1016/S1352-2310(03)00459-X, 2003.

Romer, P. S., Wooldridge, P. J., Crounse, J. D., Kim, M. J., Wennberg, P. O., Dibb, J. E., Scheuer, E., Blake, D. R., Meinardi, S., and Brosius, A. L.: Constraints on Aerosol Nitrate Photolysis as a Potential Source of HONO and NOx, Environmental science & technology, 52, 13738-13746, https://doi.org/10.1021/acs.est.8b03861, 2018.

Ryu, S. Y., Kim, J. E., Zhuanshi, H., Kim, Y. J., and Kang, G. U.: Chemical composition of post-harvest biomass burning aerosols in Gwangju, Korea, Journal of the Air & Waste Management Association, 54, 1124-1137, https://doi.org/10.1080/10473289.2004.10471018, 2004.

Sarwar, G., Roselle, S. J., Mathur, R., Appel, W., Dennis, R. L., and Vogel, B.: A comparison of CMAQ HONO predictions with observations from the Northeast Oxidant and Particle Study, Atmospheric Environment, 42, 5760-5770, https://doi.org/10.1016/j.atmosenv.2007.12.065, 2008.

Skamarock, W. C., Klemp, J. B., Dudhia, J., Gill, D. O., Barker, D. M., Duda, M. G., Huang, X.-Y., Wang, W., and Powers, J. G.: G.: A description of the Advanced Research WRF version 3, NCAR Tech. Note NCAR/TN-475+ STR, 2008.

Song, C., Chen, G., Hanna, S., Crawford, J., and Davis, D.: Dispersion and chemical evolution of ship plumes in the marine boundary layer: Investigation of O3/NOy/HOx chemistry, Journal of Geophysical Research: Atmospheres, 108, https://doi.org/10.1029/2002JD002216, 2003.

Stockwell, W. R., Middleton, P., Chang, J. S., and Tang, X.: The second generation regional acid deposition model chemical mechanism for regional air quality modeling, Journal of Geophysical Research: Atmospheres, 95, 16343-16367, https://doi.org/10.1029/JD095iD10p16343, 1990.

Su, H., Cheng, Y. F., Cheng, P., Zhang, Y. H., Dong, S., Zeng, L. M., Wang, X., Slanina, J., Shao, M., and Wiedensohler, A.: Observation of nighttime nitrous acid (HONO) formation at a non-urban site during PRIDE-PRD2004 in China, Atmospheric Environment, 42, 6219-6232, https://doi.org/10.1016/j.atmosenv.2008.04.006, 2008.

Svensson, R., Ljungström, E., and Lindqvist, O.: Kinetics of the reaction between nitrogen dioxide and water vapour, Atmospheric Environment (1967), 21, 1529-1539, https://doi.org/10.1016/0004-6981(87)90315-5, 1987.

Tao, M., Chen, L., Wang, Z., Tao, J., and Su, L.: Satellite observation of abnormal yellow haze clouds over East China during summer agricultural burning season, Atmospheric environment, 79, 632-640, https://doi.org/10.1016/j.atmosenv.2013.07.033, 2013.

Tong, S., Hou, S., Zhang, Y., Chu, B., Liu, Y., He, H., Zhao, P., and Ge, M.: Comparisons of measured nitrous acid (HONO) concentrations in a pollution period at urban and suburban Beijing, in autumn of 2014, Science China Chemistry, 58, 1393-1402, https://doi.org/10.1007/s11426-015-5454-2, 2015.

VandenBoer, T. C., Brown, S. S., Murphy, J. G., Keene, W. C., Young, C. J., Pszenny, A., Kim, S., Warneke, C., de Gouw, J. A., and Maben, J. R.: Understanding the role of the ground surface in HONO vertical structure: High resolution vertical profiles during NACHTT-11, Journal of Geophysical Research: Atmospheres, 118, 10,155-110,171, https://doi.org/10.1002/jgrd.50721, 2013.

Wang, Y., Huang, D. D., Huang, W., Liu, B., Chen, Q., Huang, R., Gen, M., Mabato, B. R. G., Chan, C. K., and Li, X.: Enhanced nitrite production from the aqueous photolysis of nitrate in the presence of vanillic acid and implications for the roles of light-absorbing organics, Environmental Science & Technology, 55, 15694-15704, https://doi.org/10.1021/acs.est.1c04642, 2021.

Weber, B., Wu, D., Tamm, A., Ruckteschler, N., Rodriguez-Caballero, E., Steinkamp, J., Meusel, H., Elbert, W., Behrendt, T., and Soergel, M.: Biological soil crusts accelerate the nitrogen cycle through large NO and HONO

878 emissions in drylands, Proceedings of the National Academy of Sciences, 112, 15384-15389,
879 https://doi.org/10.1073/pnas.1515818112, 2015.
880 Wiedinmyer, C., Akagi, S. K., Yokelson, R. J., Emmons, L. K., Al-Saadi, J. A., Orlando, J. J., and Soja, A. J.: The
881 Fire INventory from NCAR (FINN): a high resolution global model to estimate the emissions from open
882 burning, Geosci. Model Dev., 4, 625–641, https://doi.org/10.5194/gmd-4-625-2011, 2011.
883 Wiedinmyer, C., Quayle, B., Geron, C., Belote, A., McKenzie, D., Zhang, X., O'Neill, S., and Wynne, K. K.:
884 Estimating emissions from fires in North America for air quality modeling, Atmospheric Environment, 40,
885 3419-3432, https://doi.org/10.1016/j.atmosenv.2006.02.010, 2006.
886 Wiesen, P., Kleffmann, J., Kurtenbach, R., and Becker, K. H.: Mechanistic study of the heterogeneous conversion
887 of NO 2 into HONO and N 2 O on acid surfaces, Faraday Discussions, 100, 121-127,
888 https://doi.org/10.1039/FD9950000121, 1995.
889 Woo, J.-H., Kim, Y., Kim, H.-K., Choi, K.-C., Eum, J.-H., Lee, J.-B., Lim, J.-H., Kim, J., and Seong, M.:
890 Development of the CREATE Inventory in Support of Integrated Climate and Air Quality Modeling for Asia,
891 Sustainability, 12, 7930, https://doi.org/10.3390/su12197930, 2020.
892 Woo, J.-H., Choi, K.-C., Kim, H. K., Baek, B. H., Jang, M., Eum, J.-H., Song, C. H., Ma, Y.-I., Sunwoo, Y., and
893 Chang, L.-S.: Development of an anthropogenic emissions processing system for Asia using SMOKE,
894 Atmospheric environment, 58, 5-13, https://doi.org/10.1016/j.atmosenv.2011.10.042, 2012.
895 WU, D., DENG, L., LIU, Y., XI, D., ZOU, H., WANG, R., SHA, Z., PAN, Y., HOU, L., and LIU, M.: Comparisons
896 of the effects of different drying methods on soil nitrogen fractions: Insights into emissions of reactive nitrogen
897 gases (HONO and NO), Atmospheric and Oceanic Science Letters, 13, 224-231,
898 https://doi.org/10.1080/16742834.2020.1733388, 2020.
899 Xu, Z., Liu, Y., Nie, W., Sun, P., Chi, X., and Ding, A.: Evaluating the measurement interference of wet rotating-
900 denuder–ion chromatography in measuring atmospheric HONO in a highly polluted area, Atmos. Meas. Tech.,
901 12, 6737–6748, https://doi.org/10.5194/amt-12-6737-2019, 2019.
902 Xu, Z., Wang, T., Wu, J., Xue, L., Chan, J., Zha, Q., Zhou, S., Louie, P. K., and Luk, C. W.: Nitrous acid (HONO)
903 in a polluted subtropical atmosphere: Seasonal variability, direct vehicle emissions and heterogeneous
904 production at ground surface, Atmospheric environment, 106, 100-109,
905 https://doi.org/10.1016/j.atmosenv.2015.01.061, 2015.
906 Ye, C., Gao, H., Zhang, N., and Zhou, X.: Photolysis of nitric acid and nitrate on natural and artificial surfaces,
907 Environmental Science & Technology, 50, 3530-3536, https://doi.org/10.1021/acs.est.5b05032, 2016.
908 Ye, C., Zhang, N., Gao, H., and Zhou, X.: Photolysis of Particulate Nitrate as a Source of HONO and NO x,
909 Environmental Science & Technology, 51, 6849-6856, https://doi.org/10.1021/acs.est.7b00387, 2017.
910 Yuan, H., Dai, Y., Xiao, Z., Ji, D., and Shangguan, W.: Reprocessing the MODIS Leaf Area Index products for
911 land surface and climate modelling, Remote Sensing of Environment, 115, 1171-1187,
912 https://doi.org/10.1016/j.rse.2011.01.001, 2011.
913 Zhang, J., An, J., Qu, Y., Liu, X., and Chen, Y.: Impacts of potential HONO sources on the concentrations of
914 oxidants and secondary organic aerosols in the Beijing-Tianjin-Hebei region of China, Science of The Total
915 Environment, 647, 836-852, https://doi.org/10.1016/j.scitotenv.2018.08.030, 2019.
916 Zhang, J., Lian, C., Wang, W., Ge, M., Guo, Y., Ran, H., Zhang, Y., Zheng, F., Fan, X., Yan, C., Daellenbach, K.
917 R., Liu, Y., Kulmala, M., and An, J.: Amplified role of potential HONO sources in O_3 formation in North China
918 Plain during autumn haze aggravating processes, Atmos. Chem. Phys., 22, 3275–3302,
919 https://doi.org/10.5194/acp-22-3275-2022, 2022.
920 Zhang, L., Wang, T., Zhang, Q., Zheng, J., Xu, Z., and Lv, M.: Potential sources of nitrous acid (HONO) and their
921 impacts on ozone: A WRF-Chem study in a polluted subtropical region, Journal of Geophysical Research:
922 Atmospheres, 121, 3645-3662, https://doi.org/10.1002/2015JD024468, 2016.
923 Zhang, R., Sarwar, G., Fung, J. C., Lau, A. K., and Zhang, Y.: Examining the impact of nitrous acid chemistry on
924 ozone and PM over the Pearl River Delta Region, Advances in Meteorology, 2012,
925 https://doi.org/10.1155/2012/140932, 2012.

38

926 Zhang, Y., Shao, M., Lin, Y., Luan, S., Mao, N., Chen, W., and Wang, M.: Emission inventory of carbonaceous
927   pollutants from biomass burning in the Pearl River Delta Region, China, Atmospheric Environment, 76, 189-
928   199, https://doi.org/10.1016/j.atmosenv.2012.05.055, 2013.
929 Zhou, X., Zhang, N., TerAvest, M., Tang, D., Hou, J., Bertman, S., Alaghmand, M., Shepson, P. B., Carroll, M.
930   A., and Griffith, S.: Nitric acid photolysis on forest canopy surface as a source for tropospheric nitrous acid,
931   Nature Geoscience, 4, 440-443, https://doi.org/10.1038/ngeo1164, 2011.

932 Acker, K., Möller, D., Wieprecht, W., Meixner, F.X., Bohn, B., Gilge, S., Plass-Dülmer, C., Berresheim, H., 2006.
933   Strong daytime production of OH from HNO2 at a rural mountain site. Geophysical Research Letters 33.
934 Alicke, B., Geyer, A., Hofzumahaus, A., Holland, F., Konrad, S., Pätz, H., Schäfer, J., Stutz, J., Volz-Thomas, A.,
935   Platt, U., 2003. OH formation by HONO photolysis during the BERLIOZ experiment. Journal of Geophysical
936   Research: Atmospheres 108, PHO 3-1-PHO 3-17.
937 An, J., Li, Y., Chen, Y., Li, J., Qu, Y., Tang, Y., 2013. Enhancements of major aerosol components due to additional
938   HONO sources in the North China Plain and implications for visibility and haze. Advances in Atmospheric
939   Sciences 30, 57-66.
940 Binkowski, F.S., Roselle, S.J., 2003. Models-3 Community Multiscale Air Quality (CMAQ) model aerosol
941   component 1. Model description. Journal of geophysical research: Atmospheres 108.
942 Burkholder, James B., R. A. Cox, and A. R. Ravishankara. "Atmospheric degradation of ozone depleting
943   substances, their substitutes, and related species." Chemical Reviews 115.10 (2015): 3704-3759.
944 Burkholder, J. B., Sander, S. P., Abbatt, J. P. D., Barker, J. R., Cappa, C., Crounse, J. D., ... & Wine, P. H.
945   (2020). Chemical kinetics and photochemical data for use in atmospheric studies; evaluation number 19.
946   Pasadena, CA: Jet Propulsion Laboratory, National Aeronautics and Space Administration, 2020.
947 Byun, D., Schere, K.L., 2006. Review of the governing equations, computational algorithms, and other
948   components of the Models-3 Community Multiscale Air Quality (CMAQ) modeling system.
949 Carter, W.P., 2010. Development of the SAPRC-07 chemical mechanism. Atmospheric Environment 44, 5324-
950   5335.
951 Chen, F., Dudhia, J., 2001. Coupling an advanced land surface hydrology model with the Penn State NCAR
952   MM5 modeling system. Part I: Model implementation and sensitivity. Monthly weather review 129, 569-585.
953 Chen, Q., Edebeli, J., McNamara, S.M., Kulju, K.D., May, N.W., Bertman, S.B., Thanekar, S., Fuentes, J.D., Pratt,
954   K.A., 2019. HONO, Particulate Nitrite, and Snow Nitrite at a Midlatitude Urban Site during Wintertime. ACS
955   Earth and Space Chemistry 3, 811-822.
956 Cheng, Z., Wang, S., Fu, X., Watson, J.G., Jiang, J., Fu, Q., Chen, C., Xu, B., Yu, J., Chow, J.C., 2014. Impact of
957   biomass burning on haze pollution in the Yangtze River delta, China: a case study in summer 2011.
958   Atmospheric Chemistry and Physics 14, 4573-4585.
959 Colussi, A.J., Enami, S., Yabushita, A., Hoffmann, M.R., Liu, W.-G., Mishra, H., Goddard III, W.A., 2013.
960   Tropospheric aerosol as a reactive intermediate. Faraday Discussions 165, 407-420.
961 Crawford, J. H., Ahn, J. Y., Al-Saadi, J., Chang, L., Emmons, L. K., Kim, J., ... & Kim, Y. P. (2021). The
962   Korea United States air quality (KORUS-AQ) field study. Elem Sci Anth, 9(1), 00163.
963 Crutzen, P.J., Andreae, M.O., 1990. Biomass burning in the tropics: Impact on atmospheric chemistry and
964   biogeochemical cycles. Science 250, 1669-1678.
965 Czader, B., Rappenglück, B., Percell, P., Byun, D., Ngan, F., Kim, S., 2012. Modeling nitrous acid and its impact
966   on ozone and hydroxyl radical during the Texas Air Quality Study 2006. Atmospheric Chemistry & Physics
967   Discussions 12.
968 Czader, B.H., Choi, Y., Li, X., Alvarez, S., Lefer, B., 2015. Impact of updated traffic emissions on HONO mixing
969   ratios simulated for urban site in Houston, Texas. Atmospheric Chemistry and Physics 15, 1253.
970 Fu, X., Wang, T., Zhang, L., Li, Q., Wang, Z., Xia, M., Yun, H., Wang, W., Yu, C., Yue, D., 2019. The significant
971   contribution of HONO to secondary pollutants during a severe winter pollution event in southern China.
972 Gligorovski, S., 2016. Nitrous acid (HONO): An emerging indoor pollutant. Journal of Photochemistry and
973   Photobiology A: Chemistry 314, 1-5.

39

Grell, G.A., Freitas, S.R., 2014. A scale and aerosol aware stochastic convective parameterization for weather and air quality modeling. Atmos. Chem. Phys 14, 5233-5250.

Guenther, A., Jiang, X., Heald, C., Sakulyanontvittaya, T., Duhl, T., Emmons, L., Wang, X., 2012. The Model of Emissions of Gases and Aerosols from Nature version 2.1 (MEGAN2. 1): an extended and updated framework for modeling biogenic emissions.

Gutzwiller, L., Arens, F., Baltensperger, U., Gäggeler, H.W., Ammann, M., 2002. Significance of semivolatile diesel exhaust organics for secondary HONO formation. Environmental science & technology 36, 677-682.

Han, C., Yang, W., Yang, H., Xue, X., 2017. Enhanced photochemical conversion of NO2 to HONO on humic acids in the presence of benzophenone. Environmental Pollution 231, 979-986.

Hao, Q., Jiang, N., Zhang, R., Yang, L., Li, S., 2020. Characteristics, sources, and reactions of nitrous acid during winter at an urban site in the Central Plains Economic Region in China. Atmospheric Chemistry and Physics 20, 7087-7102.

Harris, G.W., Carter, W.P., Winer, A.M., Pitts, J.N., Platt, U., Perner, D., 1982. Observations of nitrous acid in the Los Angeles atmosphere and implications for predictions of ozone precursor relationships. Environmental science & technology 16, 414-419.

Hendrick, F., Müller, J.-F., Clémer, K., Wang, P., De Mazière, M., Fayt, C., Gielen, C., Hermans, C., Ma, J., Pinardi, G., 2014. Four years of ground-based MAX-DOAS observations of HONO and NO2 in the Beijing area.

Hong, S.-Y., Lim, J.-O.J., 2006. The WRF single-moment 6-class microphysics scheme (WSM6). Asia-Pacific Journal of Atmospheric Sciences 42, 129-151.

Hong, S.-Y., Noh, Y., Dudhia, J., 2006. A new vertical diffusion package with an explicit treatment of entrainment processes. Monthly weather review 134, 2318-2341.

Hou, S., Tong, S., Ge, M., An, J., 2016. Comparison of atmospheric nitrous acid during severe haze and clean periods in Beijing, China. Atmospheric environment 124, 199-206.

Hutzell, W., Luecken, D., Appel, K., Carter, W., 2012. Interpreting predictions from the SAPRC07 mechanism based on regional and continental simulations. Atmospheric Environment 46, 417-429.

Iacono, M.J., Delamere, J.S., Mlawer, E.J., Shephard, M.W., Clough, S.A., Collins, W.D., 2008. Radiative forcing by long-lived greenhouse gases: Calculations with the AER radiative transfer models. Journal of Geophysical Research: Atmospheres 113.

Jia, C., Tong, S., Zhang, W., Zhang, X., Li, W., Wang, Z., Wang, L., Liu, Z., Hu, B., Zhao, P., 2020. Pollution characteristics and potential sources of nitrous acid (HONO) in early autumn 2018 of Beijing. Science of The Total Environment 735, 139317.

Jiménez, P.A., Dudhia, J., González-Rouco, J.F., Navarro, J., Montávez, J.P., García-Bustamante, E., 2012. A revised scheme for the WRF surface layer formulation. Monthly Weather Review 140, 898-918.

Jo, Y. J., Lee, H. J., Chang, L. S., & Kim, C. H. (2017). Sensitivity Study of the Initial Meteorological Fields on the PM 10 Concentration Predictions Using CMAQ Modeling. Journal of Korean Society for Atmospheric Environment, 33(6), 554-569.

Karamchandani, P., Emery, C., Yarwood, G., Lefer, B., Stutz, J., Couzo, E., Vizuete, W., 2015. Implementation and refinement of a surface model for heterogeneous HONO formation in a 3-D chemical transport model. Atmospheric Environment 112, 356-368.

Keywood, M., Selleck, P., Reisen, F., Cohen, D., Chambers, S., Cheng, M., Cope, M., Crumeyrolle, S., Dunne, E., Emmerson, K., Fedele, R., Galbally, I., Gillett, R., Griffiths, A., Guerette, E.-A., Harnwell, J., Humphries, R., Lawson, S., Miljevic, B., Molloy, S., Powell, J., Simmons, J., Ristovski, Z., and Ward, J.: Comprehensive aerosol and gas data set from the Sydney Particle Study, Earth Syst. Sci. Data, 11, 1883–1903, https://doi.org/10.5194/essd-11-1883-2019, 2019.

Kim, S., VandenBoer, T.C., Young, C.J., Riedel, T.P., Thornton, J.A., Swarthout, B., Sive, B., Lerner, B., Gilman, J.B., Warneke, C., 2014. The primary and recycling sources of OH during the NACHTT-2011 campaign: HONO as an important OH primary source in the wintertime. Journal of Geophysical Research: Atmospheres 119, 6886-6896.

Kirchstetter, T.W., Harley, R.A., Littlejohn, D., 1996. Measurement of nitrous acid in motor vehicle exhaust. Environmental science & technology 30, 2843-2849.

40

Kleffmann, J., Gavriloaiei, T., Hofzumahaus, A., Holland, F., Koppmann, R., Rupp, L., Schlosser, E., Siese, M., Wahner, A., 2005. Daytime formation of nitrous acid: A major source of OH radicals in a forest. Geophysical Research Letters 32.

Kurtenbach, R., Becker, K., Gomes, J., Kleffmann, J., Lörzer, J., Spittler, M., Wiesen, P., Ackermann, R., Geyer, A., Platt, U., 2001. Investigations of emissions and heterogeneous formation of HONO in a road traffic tunnel. Atmospheric Environment 35, 3385-3394.

Lee, H.-J., Jo, H.-Y., Kim, J.-M., Bak, J., Park, M.-S., Kim, J.-K., Jo, Y.-J., Kim, C.-H., 2023. Nocturnal Boundary Layer Height Uncertainty in Particulate Matter Simulations during the KORUS-AQ Campaign. Remote Sensing 15, 300.

Lee, J., Whalley, L., Heard, D., Stone, D., Dunmore, R., Hamilton, J., Young, D., Allan, J., Laufs, S., Kleffmann, J., 2016. Detailed budget analysis of HONO in central London reveals a missing daytime source. Atmospheric Chemistry and Physics 16, 2747-2764.

Levy, M., Zhang, R., Zheng, J., Zhang, A.L., Xu, W., Gomez-Hernandez, M., Wang, Y., Olaguer, E., 2014. Measurements of nitrous acid (HONO) using ion drift-chemical ionization mass spectrometry during the 2009 SHARP field campaign. Atmospheric Environment 94, 231-240.

Li, D., Xue, L., Wen, L., Wang, X., Chen, T., Mellouki, A., Chen, J., Wang, W., 2018. Characteristics and sources of nitrous acid in an urban atmosphere of northern China: Results from 1-yr continuous observations. Atmospheric Environment 182, 296-306.

Li, G., Lei, W., Zavala, R., Volkamer, R., Dusanter, S., Stevens, P., Molina, L.T., 2010. Impacts of HONO sources on the photochemistry in Mexico City during the MCMA-2006/MILAGO Campaign.

Li, X., Brauers, T., Häseler, R., Bohn, B., Fuchs, H., Hofzumahaus, A., Holland, F., Lou, S., Lu, K., Rohrer, F., 2012. Exploring the atmospheric chemistry of nitrous acid (HONO) at a rural site in Southern China. Atmospheric Chemistry and Physics 12, 1497-1513.

Li, X., Rohrer, F., Hofzumahaus, A., Brauers, T., Häseler, R., Bohn, B., Broch, S., Fuchs, H., Gomm, S., Holland, F., 2014. Missing gas-phase source of HONO inferred from Zeppelin measurements in the troposphere. Science 344, 292-296.

Lu, X., Wang, Y., Li, J., Shen, L., Fung, J.C., 2018. Evidence of heterogeneous HONO formation from aerosols and the regional photochemical impact of this HONO source. Environmental Research Letters 13, 114002.

Mazzuca, G.M., Ren, X., Loughner, C.P., Estes, M., Crawford, J.H., Pickering, K.E., Weinheimer, A.J., Dickerson, R.R., 2016. Ozone production and its sensitivity to NO x and VOCs: results from the DISCOVER-AQ field experiment, Houston 2013. Atmospheric Chemistry and Physics 16, 14463-14474.

Meusel, H., Kuhn, U., Reiffs, A., Mallik, C., Harder, H., Martinez, M., Schuladen, J., Bohn, B., Parchatka, U., Crowley, J.N., 2016. Daytime formation of nitrous acid at a coastal remote site in Cyprus indicating a common ground source of atmospheric HONO and NO. Atmospheric Chemistry and Physics 16, 14475-14493.

Meusel, H., Tamm, A., Kuhn, U., Wu, D., Leifke, A.L., Fiedler, S., Ruckteschler, N., Yordanova, P., Lang-Yona, N., Pöhlker, M., 2018. Emission of nitrous acid from soil and biological soil crusts represents an important source of HONO in the remote atmosphere in Cyprus. Atmospheric Chemistry and Physics 18, 799-813.

Monks, P.S., Granier, C., Fuzzi, S., Stohl, A., Williams, M.L., Akimoto, H., Amann, M., Baklanov, A., Baltensperger, U., Bey, I., 2009. Atmospheric composition change–global and regional air quality. Atmospheric environment 43, 5268-5350.

MURPHY, Benjamin N., et al. Semivolatile POA and parameterized total combustion SOA in CMAQv5. 2: impacts on source strength and partitioning. *Atmospheric chemistry and physics*, 2017, 17.18: 11107-11133.

Nagai, K., Kubota, M., 1972. On the volatilization of nitrogen during nitrification in soils under vinyl covered culture. 5. on the effects of iron complex salts and treatments with nitrates or chloride on volatilization of nitrous acid. Jap J Sci Soil and Manure.

Nakashima, Y., Kajii, Y., 2017. Determination of nitrous acid emission factors from a gasoline vehicle using a chassis dynamometer combined with incoherent broadband cavity-enhanced absorption spectroscopy. Science of The Total Environment 575, 287-293.

41

Nie, W., Ding, A., Xie, Y., Xu, Z., Mao, H., Kerminen, V.-M., Zheng, L., Qi, X., Huang, X., Yang, X.-Q., 2015. Influence of biomass burning plumes on HONO chemistry in eastern China. Atmospheric Chemistry and Physics.

Oswald, R., Behrendt, T., Ermel, M., Wu, D., Su, H., Cheng, Y., Breuninger, C., Moravek, A., Mougin, E., Delon, C., 2013. HONO emissions from soil bacteria as a major source of atmospheric reactive nitrogen. Science 341, 1233-1235.

Pathak, R.K., Wu, W.S., Wang, T., 2009. Summertime PM 2.5 ionic species in four major cities of China: nitrate formation in an ammonia-deficient atmosphere. Atmospheric Chemistry and Physics 9, 1711-1722.

Rappenglück, B., Lubertino, G., Alvarez, S., Golovko, J., Czader, B., Ackermann, L., 2013. Radical precursors and related species from traffic as observed and modeled at an urban highway junction. Journal of the Air & Waste Management Association 63, 1270-1286.

Reisinger, A.R., 2000. Observations of HNO2 in the polluted winter atmosphere: possible heterogeneous production on aerosols. Atmospheric Environment 34, 3865-3874.

Ren, X., Harder, H., Martinez, M., Lesher, R.L., Oliger, A., Simpas, J.B., Brune, W.H., Schwab, J.J., Demerjian, K.L., He, Y., 2003. OH and HO2 chemistry in the urban atmosphere of New York City. Atmospheric Environment 37, 3639-3651.

Romer, P.S., Wooldridge, P.J., Crounse, J.D., Kim, M.J., Wennberg, P.O., Dibb, J.E., Scheuer, E., Blake, D.R., Meinardi, S., Brosius, A.L., 2018. Constraints on Aerosol Nitrate Photolysis as a Potential Source of HONO and NO x. Environmental science & technology 52, 13738-13746.

Ryu, S.Y., Kim, J.E., Zhuanshi, H., Kim, Y.J., Kang, G.U., 2004. Chemical composition of post-harvest biomass burning aerosols in Gwangju, Korea. Journal of the Air & Waste Management Association 54, 1124-1137.

Ryu, Y.-H., et al. (2022). "Role of upwind precipitation in transboundary pollution and secondary aerosol formation: A case study during the KORUS-AQ field campaign." Journal of Applied Meteorology and Climatology **61**(2): 159-174.

Sarwar, G., Roselle, S.J., Mathur, R., Appel, W., Dennis, R.L., Vogel, B., 2008. A comparison of CMAQ HONO predictions with observations from the Northeast Oxidant and Particle Study. Atmospheric Environment 42, 5760-5770.

Skamarock, W.C., Klemp, J.B., Dudhia, J., Gill, D.O., Barker, D.M., Duda, M.G., Huang, X.-Y., Wang, W., Powers, J.G., 2008. G.: A description of the Advanced Research WRF version 3, NCAR Tech. Note NCAR/TN-475+ STR. Citeseer.

Song, C., Chen, G., Hanna, S., Crawford, J., Davis, D., 2003. Dispersion and chemical evolution of ship plumes in the marine boundary layer: Investigation of O3/NOy/HOx chemistry. Journal of Geophysical Research: Atmospheres 108.

Stemmler, K., Ammann, M., Donders, C., Kleffmann, J., & George, C. (2006). Photosensitized reduction of nitrogen dioxide on humic acid as a source of nitrous acid. Nature, 440(7081), 195-198.

Stockwell, W.R., Middleton, P., Chang, J.S., Tang, X., 1990. The second generation regional acid deposition model chemical mechanism for regional air quality modeling. Journal of Geophysical Research: Atmospheres 95, 16343-16367.

Su, H., Cheng, Y.F., Cheng, P., Zhang, Y.H., Dong, S., Zeng, L.M., Wang, X., Slanina, J., Shao, M., Wiedensohler, A., 2008. Observation of nighttime nitrous acid (HONO) formation at a non-urban site during PRIDE-PRD2004 in China. Atmospheric Environment 42, 6219-6232.

Svensson, R., Ljungström, E., Lindqvist, O., 1987. Kinetics of the reaction between nitrogen dioxide and water vapour. Atmospheric Environment (1967) 21, 1529-1539.

Tao, M., Chen, L., Wang, Z., Tao, J., Su, L., 2013. Satellite observation of abnormal yellow haze clouds over East China during summer agricultural burning season. Atmospheric environment 79, 632-640.

Tong, S., Hou, S., Zhang, Y., Chu, B., Liu, Y., He, H., Zhao, P., Ge, M., 2015. Comparisons of measured nitrous acid (HONO) concentrations in a pollution period at urban and suburban Beijing, in autumn of 2014. Science China Chemistry 58, 1393-1402.

VandenBoer, T.C., Brown, S.S., Murphy, J.G., Keene, W.C., Young, C.J., Pszenny, A., Kim, S., Warneke, C., de Gouw, J.A., Maben, J.R., 2013. Understanding the role of the ground surface in HONO vertical structure:

1122   High resolution vertical profiles during NACHTT-11. Journal of Geophysical Research: Atmospheres 118,
1123   10,155-110,171.
1124 Weber, B., Wu, D., Tamm, A., Ruckteschler, N., Rodriguez-Caballero, E., Steinkamp, J., Meusel, H., Elbert, W.,
1125   Behrendt, T., Soergel, M., 2015. Biological soil crusts accelerate the nitrogen cycle through large NO and
1126   HONO emissions in drylands. Proceedings of the National Academy of Sciences 112, 15384-15389.
1127 Wiedinmyer, C., Akagi, S., Yokelson, R.J., Emmons, L., Al-Saadi, J., Orlando, J., Soja, A., 2011. The Fire
1128   INventory from NCAR (FINN): A high resolution global model to estimate the emissions from open burning.
1129   Geoscientific Model Development 4, 625.
1130 Wiedinmyer, C., Quayle, B., Geron, C., Belote, A., McKenzie, D., Zhang, X., O'Neill, S., Wynne, K.K., 2006.
1131   Estimating emissions from fires in North America for air quality modeling. Atmospheric Environment 40,
1132   3419-3432.
1133 Wiesen, P., Kleffmann, J., Kurtenbach, R., Becker, K.H., 1995. Mechanistic study of the heterogeneous conversion
1134   of NO 2 into HONO and N 2 O on acid surfaces. Faraday Discussions 100, 121-127.
1135 Woo, J.-H., Choi, K.-C., Kim, H.K., Baek, B.H., Jang, M., Eum, J.-H., Song, C.H., Ma, Y.-I., Sunwoo, Y., Chang,
1136   L.-S., 2012. Development of an anthropogenic emissions processing system for Asia using SMOKE.
1137   Atmospheric environment 58, 5-13.
1138 Woo, J.-H., Kim, Y., Kim, H.-K., Choi, K.-C., Eum, J.-H., Lee, J.-B., Lim, J.-H., Kim, J., Seong, M., 2020.
1139   Development of the CREATE Inventory in Support of Integrated Climate and Air Quality Modeling for Asia.
1140   Sustainability 12, 7930.
1141 WU, D., DENG, L., LIU, Y., XI, D., ZOU, H., WANG, R., SHA, Z., PAN, Y., HOU, L., LIU, M., 2020.
1142   Comparisons of the effects of different drying methods on soil nitrogen fractions: Insights into emissions of
1143   reactive nitrogen gases (HONO and NO). Atmospheric and Oceanic Science Letters 13, 224-231.
1144 Xu, Z., Liu, Y., Nie, W., Sun, P., Chi, X., Ding, A., 2019. Evaluating the measurement interference of wet rotating
1145   denuder ion chromatography in measuring atmospheric HONO in a highly polluted area. Atmospheric
1146   Measurement Techniques 12, 6737-6748.
1147 Xu, Z., Wang, T., Wu, J., Xue, L., Chan, J., Zha, Q., Zhou, S., Louie, P.K., Luk, C.W., 2015. Nitrous acid (HONO)
1148   in a polluted subtropical atmosphere: Seasonal variability, direct vehicle emissions and heterogeneous
1149   production at ground surface. Atmospheric environment 106, 100-109.
1150 Xue, C., Ye, C., Kleffmann, J., Zhang, C., Catoire, V., Bao, F., ... & Mu, Y. (2022). Atmospheric measurements
1151   at Mt. Tai Part I: HONO formation and its role in the oxidizing capacity of the upper boundary
1152   layer. *Atmospheric Chemistry and Physics*, 22(5), 3149-3167.
1153 Ye, C., Gao, H., Zhang, N., Zhou, X., 2016. Photolysis of nitric acid and nitrate on natural and artificial surfaces.
1154   Environmental Science & Technology 50, 3530-3536.
1155 Ye, C., Zhang, N., Gao, H., Zhou, X., 2017. Photolysis of Particulate Nitrate as a Source of HONO and NO x.
1156   Environmental Science & Technology 51, 6849-6856.
1157 Yu, Chuan, et al. "Measurement of heterogeneous uptake of NO2 on inorganic particles, sea water and urban
1158   grime." Journal of Environmental Sciences 106 (2021): 124-135.
1159 Yu, C., Huang, L., Xue, L., Shen, H., Li, Z., Zhao, M., ... & Wang, W. (2022). Photoenhanced heterogeneous
1160   uptake of NO2 and HONO formation on authentic winter time urban grime. *ACS Earth and Space
1161   Chemistry*, 6(8), 1960-1968.
1162 Yuan, H., Dai, Y., Xiao, Z., Ji, D., Shangguan, W., 2011. Reprocessing the MODIS Leaf Area Index products for
1163   land surface and climate modelling. Remote Sensing of Environment 115, 1171-1187.
1164 Zhang, J., An, J., Qu, Y., Liu, X., Chen, Y., 2019. Impacts of potential HONO sources on the concentrations of
1165   oxidants and secondary organic aerosols in the Beijing-Tianjin-Hebei region of China. Science of The Total
1166   Environment 647, 836-852.
1167 Zhang, J., Lian, C., Wang, W., Ge, M., Guo, Y., Ran, H., Zhang, Y., Zheng, F., Fan, X., Yan, C., 2022. Amplified
1168   role of potential HONO sources in O 3 formation in North China Plain during autumn haze aggravating
1169   processes. Atmospheric Chemistry and Physics 22, 3275-3302.

1170   Zhang, L., Wang, T., Zhang, Q., Zheng, J., Xu, Z., Lv, M., 2016. Potential sources of nitrous acid (HONO) and
1171   their impacts on ozone: A WRF-Chem study in a polluted subtropical region. Journal of Geophysical Research:
1172   Atmospheres 121, 3645-3662.
1173   Zhang, R., Sarwar, G., Fung, J.C., Lau, A.K., Zhang, Y., 2012. Examining the impact of nitrous acid chemistry on
1174   ozone and PM over the Pearl River Delta Region. Advances in Meteorology 2012.
1175   Zhang, Y., Shao, M., Lin, Y., Luan, S., Mao, N., Chen, W., Wang, M., 2013. Emission inventory of carbonaceous
1176   pollutants from biomass burning in the Pearl River Delta Region, China. Atmospheric Environment 76, 189-
1177   199.
1178   Zhou, X., Zhang, N., TerAvest, M., Tang, D., Hou, J., Bertman, S., Alaghmand, M., Shepson, P.B., Carroll, M.A.,
1179   Griffith, S., 2011. Nitric acid photolysis on forest canopy surface as a source for tropospheric nitrous acid.
1180   Nature Geoscience 4, 440-443.

1181

An investigation into atmospheric nitrous acid (HONO) processes in South Korea

Kiyeon Kim[1], Kyung M. Han[1]*, Chul H. Song[1]*, Hyojun Lee[1], Ross Beardsley[2], Jinhyeok Yu[1], Greg Yarwood[2], Bonyoung Koo[3], Jasper Madalipay[1], Jung-Hun Woo[4], and Seogju Cho[5]

1. School of Earth Sciences and Environmental Engineering, Gwangju Institute of Science and Technology (GIST), Gwangju 61005, Republic of Korea

2. Ramboll USA, Novato, CA 94945, USA

3. Bay Area Air Quality Management District, San Francisco, CA 94105, USA

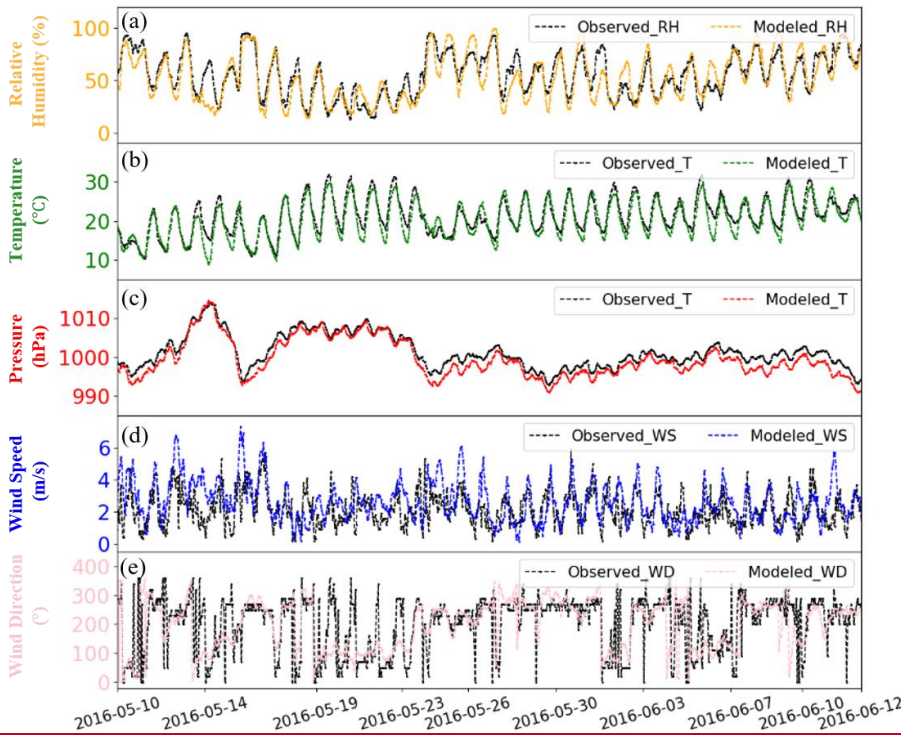4. Department of Technology Fusion Engineering, College of Engineering, Konkuk University, Seoul 05029, Republic of Korea

5. Seoul Metropolitan Government Research Institute of Public Health Environment, 30, Janggunmaeul 3-gil, Gwacheon-si, Gyeonggi-do 13818, Republic of Korea

* **Corresponding authors:** Kyung Man Han (kmhan@gist.ac.kr) and Chul Han Song (chsong@gist.ac.kr)
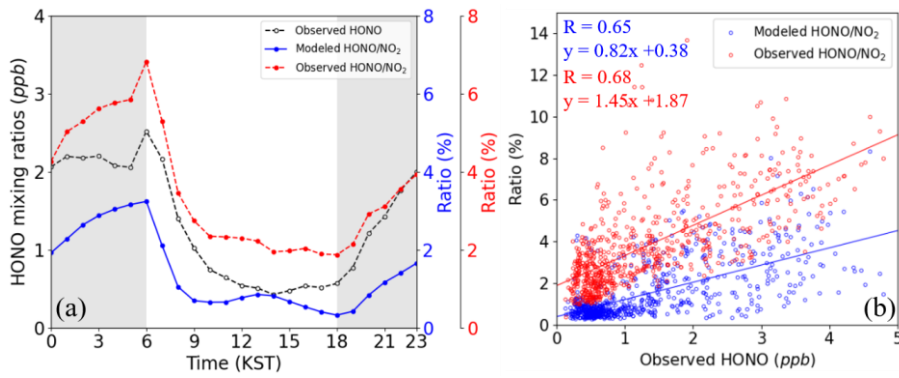
1202

Fig. S1. Temporal variations of (a) relative humidity (RH); (b) temperature (T); (c) pressure; (d) wind speed (WS) at 10m above the surface; and (e) wind direction (WD) at 10m above the surface during period of the KORUS-AQ campaign.

1203

1204

1205

1206

서식 있음: 캡션, 왼쪽

Fig. ~~S1~~S2. (a) Diurnal variations of observed HONO (black open circles, left y-axis), modeled HONO to NO_2 ratio (blue line, right y-axis), and observed HONO to NO_2 ratio (red line, right y-axis) and (b) their scatter-plots between the observed HONO and the modeled ratio of HONO to NO_2 (blue circles), and observed HONO to NO_2 (red circles) at the Olympic Park station during the period of the KORUS-AQ campaign.

47
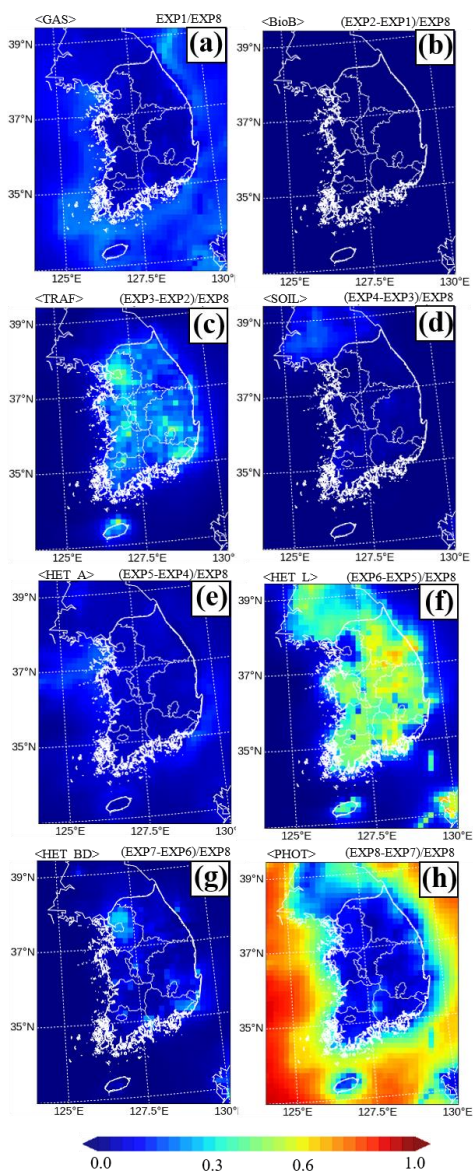
1213

Fig. ~~S2~~S3. Incremental ratio of (a) gas phase reactions; (b) biomass burning emissions; (c) traffic emissions and (d) soil emissions; (e) heterogeneous reactions on the aerosol surfaces, (f) heterogeneous reactions on the leaf surfaces, and (g) heterogeneous reactions on the building surfaces; and (h) renoxification on HONO mixing ratios (unit: dimensionless).

1218
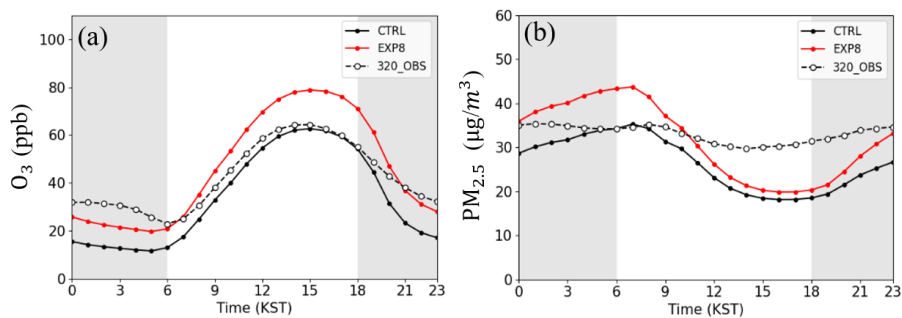
Fig. ~~S4~~S4. Comparison of diurnal variations of the mixing ratios of (a) O_3, and (b) $PM_{2.5}$. Both are averaged for 320 AIR KOREA monitoring stations during the period of the KORUS-AQ campaign. The black open circles, black lines, and red lines represent observed values and values from the CTRL and EXP8 simulations, respectively.
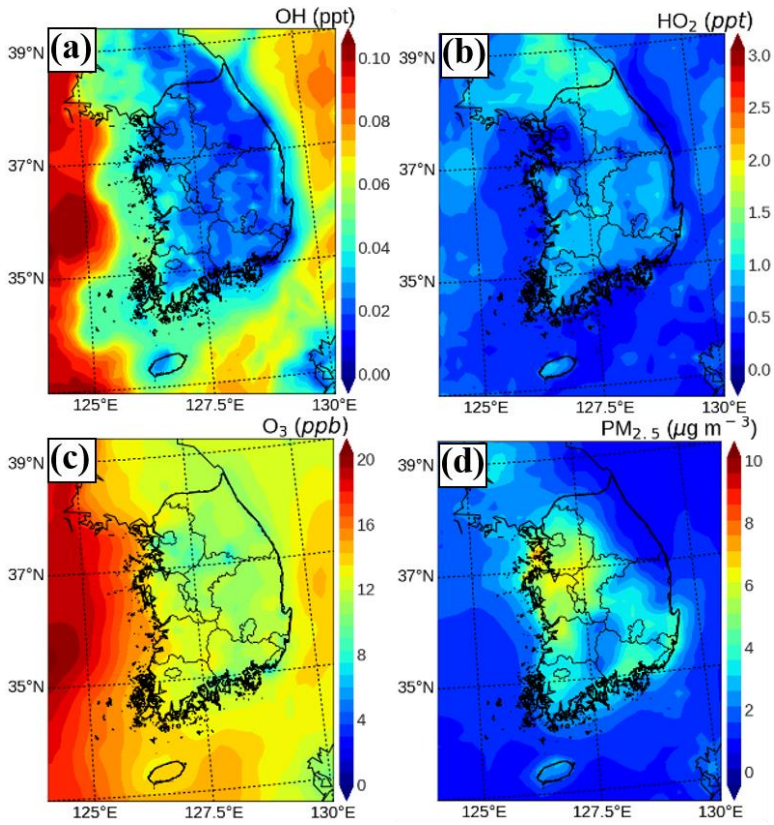
1223

1224 **Fig. ~~S5~~S5.** Spatial distributions of the differences levels of (a) HONO, (b) OH, (c) HO$_2$, and
1225 (d) PM$_{2.5}$ between the EXP8 and CTRL simulations in South Korea during the period of the
1226 KORUS-AQ campaign.

1227 **Table S1.** Detection limits and uncertainties of instruments for observed HONO, NO_2, O_3, and
1228 $PM_{2.5}$ at Olympic Park station, Korea.

Species	Instruments	Detection limit	Uncertainty	Time resolution
HONO	Monitor for Aerosols and Gases in Ambient Air (MARGA, model ADI 2080)	0.02ppbv	±20%	1 hour
NO_2	Ecotech gas sensor, EC8941	0.5ppbv	±10%	1 hour
O_3	Ecotech gas sensor, EC9810	0.5ppbv	±5%	1 hour
$PM_{2.5}$	Thermo Fisher Scientific, FH62C14	$4\mu g/m^3$	±10%	1 hour

1229

1230 **Table S2**. Statistical analysis of modeled and observed meteorological parameters at the
1231 Olympic Park station during the period of the KORUS-AQ campaign.

Parameter	Observed mean	Modeled mean	R	RMSE	MB	IOA
RH (%)	55.81	53.33	0.85	11.95	-2.48	0.92
	55.50	55.60	0.87	11.06	0.09	0.93
T (℃)	21.27	20.28	0.93	1.96	-0.99	0.96
	22.38	21.10	0.94	1.84	-1.28	0.94
Pressure (hPa)	1001.38	999.62	0.98	2.01	-1.77	0.95
	1000.35	999.75	0.97	1.14	-0.60	0.98
WS (m s^{-1})	2.14	2.65	0.47	1.30	0.51	0.66
	2.08	2.46	0.45	1.17	0.39	0.65
WD (°)	202.71	196.01	0.53	88.87	-6.70	0.75
	205.40	202.18	0.53	83.49	-3.24	0.74

1232